

ARTICLE

Human germline heterozygous gain-of-function *STAT6* variants cause severe allergic disease

Mehul Sharma^{1*}, Daniel Leung^{2*}, Mana Momenilandi^{3,4*}, Lauren C.W. Jones^{1**}, Lucia Pacillo^{5,6,7**}, Alyssa E. James^{8**}, Jill R. Murrell^{9**}, Selket Delafontaine^{10,11**}, Jesmeen Maimaris^{12,13**}, Maryam Vaseghi-Shanjani^{1**}, Kate L. Del Bel^{1**}, Henry Y. Lu^{14,15,16**}, Gilbert T. Chua^{2,17}, Silvia Di Cesare^{5,7}, Oriol Fornes^{18,19}, Zhongyi Liu², Gigliola Di Matteo^{6,7}, Maggie P. Fu^{20,21}, Donato Amodio⁶, Issan Yee San Tam², Gavin Shueng Wai Chan²², Ashish A. Sharma²³, Joshua Dalmann¹, Robin van der Lee^{18,19}, Géraldine Blanchard-Rohner^{1,24}, Susan Lin¹, Quentin Philippot^{3,4}, Phillip A. Richmond^{11,18}, Jessica J. Lee^{18,25}, Allison Matthews^{18,26}, Michael Seear¹, Alexandra K. Turvey¹, Rachael L. Philips²⁷, Terri F. Brown-Whitehorn²⁸, Christopher J. Gray²⁹, Kosuke Izumi²⁹, James R. Treat³⁰, Kathleen H. Wood⁹, Justin Lack³¹, Asya Khleborodova³¹, Julie E. Niemela³², Xingtian Yang², Rui Liang², Lin Kui^{2,33}, Christina Sze Man Wong³⁴, Grace Wing Kit Poon³⁵, Alexander Hoischen³⁶, Caspar I. van der Made³⁶, Jing Yang², Koon Wing Chan², Jaime Sou Da Rosa Duque², Pamela Pui Wah Lee², Marco Hok Kung Ho^{2,37}, Brian Hon Yin Chung², Huong Thi Minh Le³⁸, Wanling Yang², Pejman Rohani³⁹, Ali Fouladvand⁴⁰, Hassan Rokni-Zadeh⁴¹, Majid Changi-Ashtiani⁴², Mohammad Miryounesi⁴³, Anne Puel^{3,4,60}, Mohammad Shahrooei⁴⁴, Andrea Finocchi^{5,7}, Paolo Rossi^{5,45}, Beatrice Rivalta^{5,6,7}, Cristina Cifaldi⁷, Antonio Novelli⁴⁶, Chiara Passarelli⁴⁶, Stefania Arasi⁴⁷, Dominique Bullens^{48,49}, Kate Sauer^{50,51}, Tania Claeys⁵², Catherine M. Biggs¹, Emma C. Morris^{12,13}, Sergio D. Rosenzweig³², John J. O’Shea²⁷, Wyeth W. Wasserman¹⁸, H. Melanie Bedford^{26,53}, Clara D.M. van Karnebeek^{18,54}, Paolo Palma^{5,6}, Siobhan O. Burns^{12,13***}, Isabelle Meyts^{10,11***}, Jean-Laurent Casanova^{3,4,55,56,60***}, Jonathan J. Lyons^{8***}, Nima Parvaneh^{57***}, Anh Thi Van Nguyen^{58***}, Caterina Cancrini^{5,7***}, Jennifer Heimall^{28***}, Hanan Ahmed^{59***}, Margaret L. McKinnon^{19***}, Yu Lung Lau^{2***}, Vivien Béziat^{3,4,60***}, and Stuart E. Turvey^{1***}

STAT6 (signal transducer and activator of transcription 6) is a transcription factor that plays a central role in the pathophysiology of allergic inflammation. We have identified 16 patients from 10 families spanning three continents with a profound phenotype of early-life onset allergic immune dysregulation, widespread treatment-resistant atopic dermatitis, hypereosinophilia with eosinophilic gastrointestinal disease, asthma, elevated serum IgE, IgE-mediated food allergies, and anaphylaxis. The cases were either sporadic (seven kindreds) or followed an autosomal dominant inheritance pattern (three kindreds). All patients carried monoallelic rare variants in *STAT6* and functional studies established their gain-of-function (GOF) phenotype with sustained *STAT6* phosphorylation, increased *STAT6* target gene expression, and T_H2 skewing. Precision treatment with the anti-IL-4Rα antibody, dupilumab, was highly effective improving both clinical manifestations and immunological biomarkers. This study identifies heterozygous GOF variants in *STAT6* as a novel autosomal dominant allergic disorder. We anticipate that our discovery of multiple kindreds with germline *STAT6* GOF variants will facilitate the recognition of more affected individuals and the full definition of this new primary atopic disorder.

Introduction

Asthma and related atopic diseases, including atopic dermatitis, food allergy, allergic rhinitis, and eosinophilic gastrointestinal diseases, are estimated to affect ~20% of the global population imposing immense health and economic burdens (Dierick et al., 2020). Identifying human single-gene defects that lead to severe allergic disease—so-called primary atopic disorders (PADs)—is a powerful strategy to define the cellular and molecular mechanisms that drive human allergic inflammation (Lyons and Milner, 2018;

Vaseghi-Shanjani et al., 2021). Identifying new PADs accelerates the diagnosis and treatment of affected individuals and can uncover new molecular targets for preventing and treating common allergic disease.

Currently there are only a few known inborn errors of immunity (IEIs) underlying severe allergic disease (Milner, 2020). Indeed, most cases are of unknown etiology, particularly those that are isolated or sporadic. In this study, we describe a novel human PAD caused by germline heterozygous gain-of-function

*M. Sharma, D. Leung, and M. Momenilandi contributed equally to this paper; **L.C.W. Jones, L. Pacillo, A.E. James, J.R. Murrell, S. Delafontaine, J. Maimaris, M. Vaseghi-Shanjani, K.L. Del Bel, and H.Y. Lu contributed equally to this paper; ***S.O. Burns, I. Meyts, J.L. Casanova, J.J. Lyons, N. Parvaneh, A.T.V. Nguyen, C. Cancrini, J. Heimall, H. Ahmed, and M.L. McKinnon contributed equally to this paper; ****Y.L. Lau, V. Béziat, and S.E. Turvey contributed equally to this paper. Correspondence to Stuart E. Turvey: sturvey@cw.bc.ca; Mehul Sharma: msharma@bccr.ca.



¹Dept. of Pediatrics, BC Children's Hospital, University of British Columbia, Vancouver, Canada; ²Dept. of Paediatrics and Adolescent Medicine, School of Clinical Medicine, The University of Hong Kong, Hong Kong, China; ³Laboratory of Human Genetics of Infectious Diseases, Necker Branch, INSERM, Necker Hospital for Sick Children, Paris, France; ⁴Imagine Institute, University of Paris-Cité, Paris, France; ⁵Dept. of System Medicine, Pediatric Chair, University of Tor Vergata, Rome, Italy; ⁶Academic Dept. of Pediatrics (DPUO), Unit of Clinical Immunology and Vaccinology, IRCCS Bambin Gesù Children Hospital, Rome, Italy; ⁷Research Unit of Primary Immunodeficiency, IRCCS Bambin Gesù Children Hospital, Rome, Italy; ⁸Translational Allergic Immunopathology Unit, Laboratory of Allergic Diseases, National Institute of Allergy and Infectious Diseases (NIAID), National Institutes of Health (NIH), Bethesda, MD, USA; ⁹Pathology and Laboratory Medicine, Division of Genomic Diagnostics, Children's Hospital of Philadelphia, Philadelphia, PA, USA; ¹⁰Dept. of Microbiology, Immunology and Transplantation, Laboratory for Inborn Errors of Immunity, KU Leuven, Leuven, Belgium; ¹¹Dept. of Pediatrics, Pediatric Immunodeficiencies Division, University Hospitals Leuven, Leuven, Belgium; ¹²Institute of Immunity and Transplantation, Division of Infection and Immunity, University College London, London, UK; ¹³Dept. of Immunology, Royal Free London NHS Foundation Trust, London, UK; ¹⁴Division of Hematology/Oncology, Boston Children's Hospital, Harvard Medical School, Boston, MA, USA; ¹⁵Dept. of Pediatric Oncology, Dana-Farber Cancer Institute, Harvard Medical School, Boston, MA, USA; ¹⁶Broad Institute of Massachusetts Institute of Technology and Harvard, Cambridge, MA, USA; ¹⁷Allergy Centre, Union Hospital, Hong Kong, China; ¹⁸Centre for Molecular Medicine and Therapeutics, BC Children's Hospital Research Institute, Vancouver, Canada; ¹⁹Dept. of Medical Genetics, University of British Columbia, Vancouver, Canada; ²⁰Dept. of Medical Genetics, The University of British Columbia, Vancouver, Canada; ²¹Genome Science and Technology Program, Faculty of Science, The University of British Columbia, Vancouver, Canada; ²²Dept. of Pathology, Queen Mary Hospital, Hong Kong, China; ²³Dept. of Pathology, Emory University, Atlanta, GA, USA; ²⁴Unit of Immunology and Vaccinology, Division of General Pediatrics, Dept. of Woman, Child, and Adolescent Medicine, Geneva University Hospitals and Faculty of Medicine, University of Geneva, Geneva, Switzerland; ²⁵Genome Science and Technology Graduate Program, University of British Columbia, Vancouver, Canada; ²⁶Dept. of Paediatrics, University of Toronto, Toronto, Canada; ²⁷Molecular Immunology and Inflammation Branch, National Institute of Arthritis, Musculoskeletal and Skin Diseases, NIH, Bethesda, MD, USA; ²⁸Dept. of Pediatrics, Division of Allergy and Immunology, Children's Hospital of Philadelphia, Philadelphia, PA, USA; ²⁹Pediatrics, Division of Human Genetics, Children's Hospital of Philadelphia, Philadelphia, PA, USA; ³⁰Pediatrics, Division of Pediatric Dermatology, Perelman School of Medicine, University of Pennsylvania, Philadelphia, PA, USA; ³¹NIAID Collaborative Bioinformatics Resource, NIAID, NIH, Bethesda, MD, USA; ³²Immunology Service, Clinical Center, NIH, Bethesda, MD, USA; ³³Dept. of Pediatrics, University of California San Diego, La Jolla, CA, USA; ³⁴Dept. of Medicine, Division of Dermatology, The University of Hong Kong, Hong Kong, China; ³⁵Dept. of Paediatrics and Adolescent Medicine, Queen Mary Hospital, Hong Kong, China; ³⁶Dept. of Human Genetics, Radboud University Medical Center, Nijmegen, Netherlands; ³⁷Virtus Medical, Hong Kong, China; ³⁸Pediatric Center, Vinmec Times City International General Hospital, Hanoi, Vietnam; ³⁹Pediatrics, Pediatric Gastroenterology and Hepatology Research Center, Pediatrics Centre of Excellence, Children's Medical Center, University of Medical Sciences, Tehran, Iran; ⁴⁰Pediatrics, Allergy and Clinical Immunology, Lorestan University of Medical Sciences, Khoramabad, Iran; ⁴¹Dept. of Medical Biotechnology, School of Medicine, Zanjan University of Medical Sciences, Zanjan, Iran; ⁴²School of Mathematics, Institute for Research in Fundamental Sciences, Tehran, Iran; ⁴³Dept. of Medical Genetics, School of Medicine, Shahid Beheshti University of Medical Sciences, Tehran, Iran; ⁴⁴Microbiology and Immunology, Laboratory of Clinical Bacteriology and Mycology, KU Leuven, Leuven, Belgium; ⁴⁵DPUO, Research Unit of Infectivology and Pediatrics Drugs Development, Bambino Gesù Children Hospital IRCCS, Rome, Italy; ⁴⁶Laboratory of Medical Genetics, Translational Cytogenomics Research Unit, Bambino Gesù Children Hospital IRCCS, Rome, Italy; ⁴⁷Allergy Unit, Area of Translational Research in Pediatric Specialties, Bambino Gesù Children's Hospital, IRCCS, Rome, Italy; ⁴⁸Dept. of Microbiology, Immunology and Transplantation, Allergy and Clinical Immunology Research Group, KU Leuven, Leuven, Belgium; ⁴⁹Dept. of Pediatrics, Pediatric Allergy Division, University Hospitals Leuven, Leuven, Belgium; ⁵⁰Dept. of Pediatrics, Pediatric Pulmonology Division, AZ Sint-Jan Brugge, Brugge, Belgium; ⁵¹Dept. of Pediatrics, Pediatric Pulmonology Division, University Hospitals Leuven, Leuven, Belgium; ⁵²Dept. of Pediatrics, Pediatric Gastroenterology Division, AZ Sint-Jan Brugge, Brugge, Belgium; ⁵³Genetics Program, North York General Hospital, Toronto, Canada; ⁵⁴Depts. of Pediatrics and Clinical Genetics, Amsterdam University Medical Centers, Amsterdam, Netherlands; ⁵⁵Howard Hughes Medical Institute, The Rockefeller University, New York, NY, USA; ⁵⁶Department of Pediatrics, Necker Hospital for Sick Children, AP-HP, France; ⁵⁷Department of Pediatrics, Children's Medical Center, Tehran University of Medical Sciences, Tehran, Iran; ⁵⁸Dept. of Immunology, Allergy and Rheumatology, Division of Primary Immunodeficiency, Vietnam National Children's Hospital, Hanoi, Vietnam; ⁵⁹Faculty of Health Sciences, McMaster University, Hamilton, Canada; ⁶⁰St. Giles Laboratory of Human Genetics of Infectious Diseases, Rockefeller Branch, The Rockefeller University, New York, NY, USA.

(GOF) variants in the gene *STAT6* found in 16 individuals from 10 unrelated families spanning three continents. Signal transducer and activator of transcription 6 (*STAT6*) is the main transcription factor that mediates the biological effects of IL-4, a key cytokine necessary for type 2 differentiation of T cells, B cell survival, proliferation, and class switching to IgE (Goenka and Kaplan, 2011; Takeda et al., 1996; Villarino et al., 2020; Villarino et al., 2017), as well as that of IL-13, a cytokine linked to anaphylaxis (Gowthaman et al., 2019). Affected individuals experienced early-onset severe, sometimes fatal, multisystem allergic disease which was refractory to conventional treatments. Notably, precision therapeutics aimed at targeting exaggerated *STAT6* signaling were beneficial in those who received them.

Results

Identification of 16 patients from 10 families with severe early-onset allergic disease heterozygous for rare damaging *STAT6* variants

We studied 16 patients from 10 kindreds with severe early-onset allergic disease spanning three continents. Patients were identified by their expert clinicians as candidates for genetic assessment based on their extreme phenotype and, in some cases, their family history (see clinical narratives in Data S1; Tables S4

and S5; and Fig. 1 A). The patients were from diverse ethnicities, specifically European (Kindred D, F, and J), Middle Eastern (Kindred A and C), Hispanic (Kindred B), South Asian (Kindred H), East Asian (Kindred E), and Southeast Asian (Kindred Y). The cases were either sporadic (seven kindreds) or affected multiple individuals of either sex over different generations consistent with autosomal dominant (AD) inheritance (Kindreds C, F, and J). All patients carried monoallelic rare variants in *STAT6* (NM_001178079.2). The consensus negative selection score of *STAT6* reveals a negative selection score that overlaps with known AD IEIs (Rapaport et al., 2021), consistent with the AD inheritance pattern observed in Kindreds C, F, and J (Fig. 1 B). In addition, and also consistent with an AD disorder, by sequencing both healthy parents (when available) we established that the *STAT6* mutation was de novo in Patient 2 (P2), P5, P10, and P12 (from Kindreds B, D, G, and I, respectively; Fig. 1 A). The disease was fully penetrant in the families studied, as all *STAT6* variant carriers were affected. None of the variants have previously been reported in population databases (Fig. 1 C; i.e., gnomAD). All the variants were private to the studied kindreds, except the p.D419G variant which was common in Kindreds A and E. Pathogenicity prediction models identify all of these variants to be pathogenic, evidenced by high pathogenic CADD (Rentzsch et al., 2021), SIFT (Sim et al., 2012), and Polyphen-2 (Adzhubei et al., 2010) scores (Tables S4 and S5).

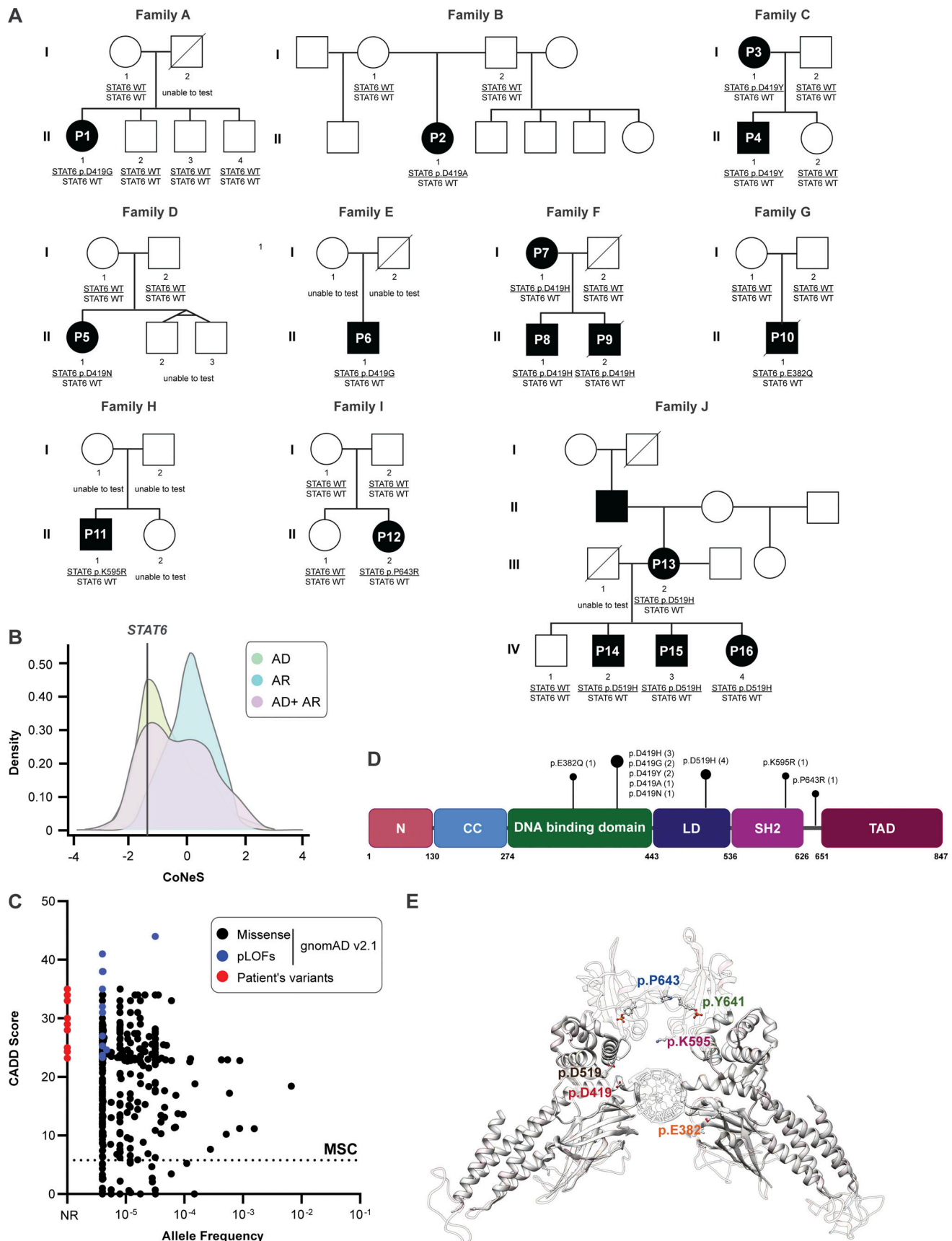


Figure 1. **16 patients with severe allergic disease and STAT6 variants in different protein domains.** (A) Family pedigree of the 16 patients from 10 different families. Filled symbols = affected individual; unfilled symbols = unaffected individual. (B) Consensus negative selection (CoNeS) score for STAT6 in

relation to the score for known IEI genes reported with inheritance pattern of either AD, AR, or both (AD + AR). **(C)** Frequency and CADD score for missense (black) and predicted LOF (pLOF, blue) *STAT6* variants reported in a public database and *STAT6* variants reported in our patient cohort (red). The dotted line corresponds to the mutation significance cutoff (MSC). **(D)** Schematic illustrating the protein domains of *STAT6*. Amino acid location of the variants shown are highlighted, with the length of the bar corresponding to the number of patients reported with variants at that site. **(E)** Structural model of the DNA-*STAT6* homodimer complex showing location of the different *STAT6* variants in relation to the DNA-binding interface.

Remarkably, nine patients from six kindreds carried a variant affecting amino acid D419. Importantly, variants leading to amino acid changes at p.D419, p.D519, and p.P643 can be found in the Catalogue of Somatic Mutations in Cancer (COSMIC) database as recurrent somatic variants in lymphoma with some experimental evidence for a GOF phenotype for variants at p.D419 (Yildiz et al., 2015; Zamò et al., 2018; Fig. S1 A). The reported variants lie in different protein domains of *STAT6*, including the DNA-binding domain (p.E382 and p.D419), the linker domain (p.D519), and the SH2 domain (p.K595), while p.P643 lies in close proximity to the p.Y641 phosphorylation site (Fig. 1, D–E). Although the variants were located within different domains of the *STAT6* protein, modeling of *STAT6* interacting with DNA reveals that all the identified variants (with the exception of p.P643) lie near the protein–DNA interface and result in amino acid changes leading to increased electro-positivity at physiological pH (Fig. 1 E). Notably, E382 and D419 are located in regions responsible for protein–DNA recognition (Li et al., 2016). Changes in these variants decrease the electro-negativity of the protein near the DNA-binding interface and are predicted to enhance *STAT6* binding to DNA (Fig. 1 E and Fig. S1 B). In aggregate, these data suggest that the *STAT6* germline monoallelic variants identified in the patients underlie severe allergic disease by a GOF mechanism.

Unifying clinical features of the 16 patients with severe allergic disease

The patients in the cohort were aged from 3 to 60 yr. Full clinical narratives are provided in Data S1, and their clinical features are summarized in Fig. 2 A. All had severe allergic disease which began in their first year of life. Severe, treatment-resistant atopic dermatitis (15/16) and food allergies (15/16) were the most common clinical manifestations, followed by asthma (11/16) and eosinophilic gastrointestinal disease (10/16) and severe episodes of anaphylaxis (9/16). Clinical laboratory testing was notable for eosinophilia and markedly elevated serum IgE levels (Fig. 2, B and C). Other aspects of the clinical laboratory and immunological work up were largely unremarkable, although clinical hallmarks of chronic systemic inflammation were present in some patients (i.e., elevations in white blood cell counts, platelets, and serum immunoglobulin levels). T, B, and natural killer (NK) cell numbers were all typically in the normal range (Fig. S2). Clinical biopsies confirmed the presence of eosinophils in the skin and gastrointestinal tract (Fig. 2, E–G). Endoscopic visualization of the esophagus revealed trachealization and furrowing consistent with eosinophilic esophagitis (Bolton et al., 2018; Fig. 2, H and I).

In addition to atopic disease, half of the patients presented with recurrent skin, respiratory, and viral infections, although there were no deep-seated or fatal infections. Short stature (less than third percentile for age) was a common feature (7/16), and

5/16 had other skeletal issues such as pathologic fractures and generalized hypermobility. Finally, two of the patients died from their disease; one from anaphylaxis at the age of 20 yr and another from a cerebral aneurysm at age 35 yr. These clinical presentations highlight the severity of the multi-system disease found in this patient cohort.

Functional analysis of the *STAT6* variants confirms their GOF activity

To assess the functional impact of the *STAT6* variants, we selected HEK293 cells as our model system, as these cells lack endogenous *STAT6* but express other components of the IL-4R pathway (Fig. 3 A; Mikita et al., 1996). HEK293 cells were transfected with each of the 10 patient *STAT6* variants along with three different controls: WT *STAT6*, a predicted damaging *STAT6* population variant found in the gnomAD healthy population database (p.A321V), and a biochemically inactive *STAT6* variant (p.Y641F; Wick and Berton, 2000). To investigate *STAT6* transcription factor activity, we conducted luciferase assays with three different reporter plasmids containing *STAT6* binding sites (Li et al., 2016). While there were some differences related to the specific combinations of reporter plasmids and patient variants, there was evidence of GOF activity with all *STAT6* patient variants resulting in higher promoter activity at baseline and after stimulation compared to the controls (Fig. 3 B and Fig. S3, A and B). The phosphorylation status of *STAT6* variants was also quantified by flow cytometry and was confirmed to be higher at baseline and after stimulation compared to WT (Fig. 3, C and D; and Fig. S3 C). *STAT6* phosphorylation was not detectable by flow cytometry for the p.P643R variant; however, increased baseline phosphorylation was confirmed by immunoblotting (Fig. 3 E and Fig. S3, D and E). This may point to a conformational change in tertiary structure of *STAT6* near the phosphorylation site p.Y641 for this variant that rendered it inaccessible to the flow cytometry antibody.

We next evaluated if the increased promoter activity leads to global transcriptomic changes. As transcriptomic studies on HEK293 cells after IL-4 stimulation have been challenging to interpret (Yildiz et al., 2015), we stably expressed p.E382Q and p.D419G *STAT6* by lentiviral transduction in Jurkat T cells, which express endogenous *STAT6* and serve as a model of heterozygosity (Kim et al., 2012). Here, we observed that WT-, p.E382Q-, and p.D419G-transduced cells clustered separately from each other both at baseline and after stimulation with IL-4 (Fig. 3 F). Differential gene expression analysis revealed significantly increased transcript abundance of known *STAT6* target genes, including *IL4R* (Goenka and Kaplan, 2011), *CISH* (Yildiz et al., 2015), and *XBPI* (Bettigole et al., 2015) in p.E382Q and p.D419G transduced cells when compared to WT transduced control (Fig. 3 G). Interestingly, p.E382Q and p.D419G had 67 and

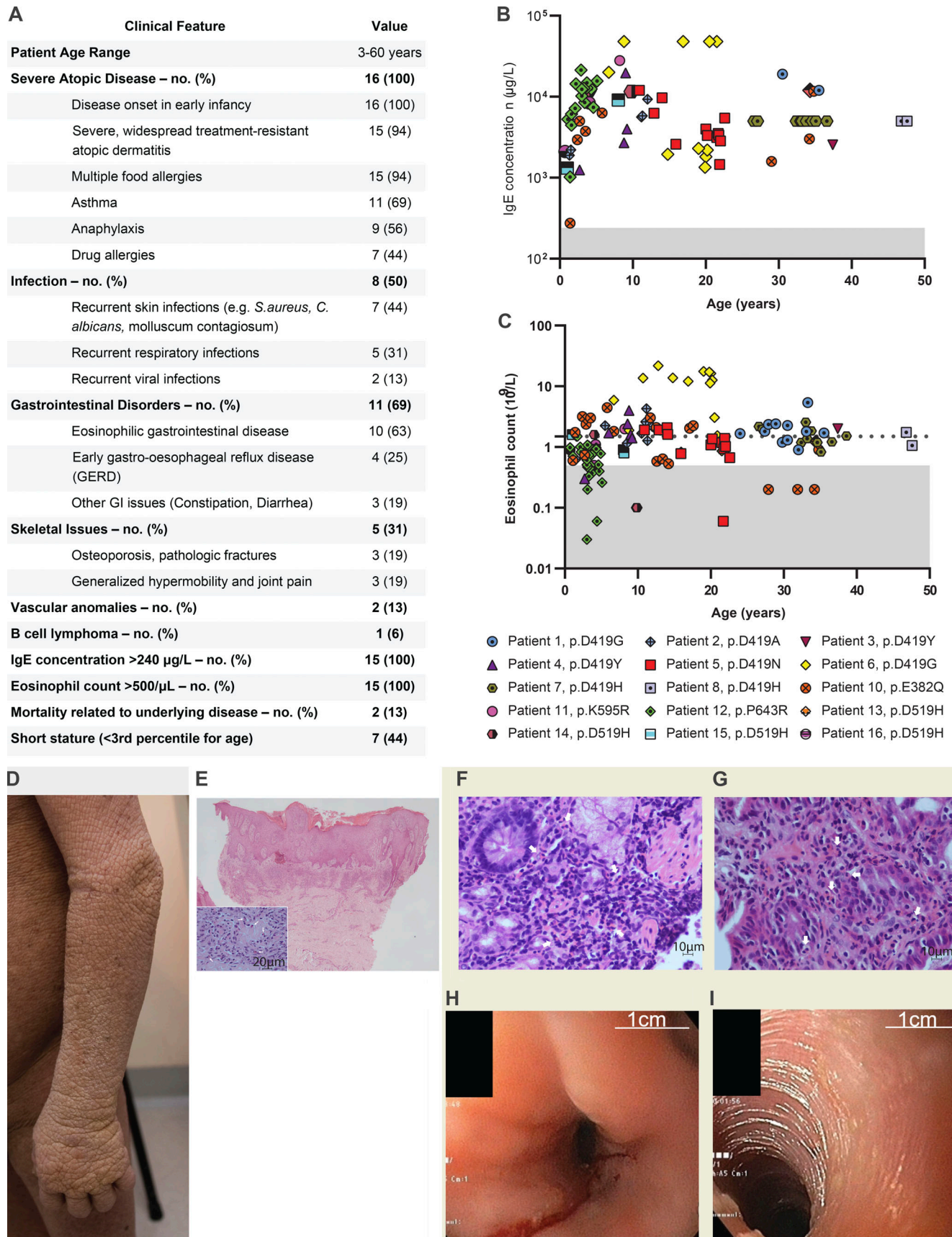


Figure 2. **Major clinical features of the 16 patients.** (A) Tabulation and comparison of the clinical phenotype for 16 patients. Please note blood eosinophil and IgE values were only available for 15 patients. (B) IgE concentration in whole blood for 15 out of the 16 patients. Shaded area represents IgE < 240 µg/liter,

which is the typical upper limit of normal. **(C)** Eosinophil count in whole blood for 15 out of the 16 patients. Shaded area represents counts $<0.5 \times 10^9$ /liter, which is the typical upper limit of normal. The horizontal broken line denotes an eosinophil count of 1.5×10^9 /liter, since hypereosinophilic syndrome is traditionally defined as peripheral blood eosinophilia $>1.5 \times 10^9$ /liter persisting ≥ 6 mo. **(D)** Photograph of widespread and severe atopic disease. **(E)** Photomicrograph of the skin biopsy showing marked pseudoepitheliomatous hyperplasia with acanthosis, hyperkeratosis, and focal parakeratosis, suggestive of lichen simplex chronicus (H&E stain, original magnification 2 \times). Moderate chronic inflammation within the papillary dermis in which scattered eosinophils (white arrows) are conspicuous (inset, H&E stain; original magnification, 40 \times). **(F)** Photomicrograph of duodenal biopsy showing abundant eosinophils (white arrows) amongst lymphocytes (H&E stain; original magnification, 40 \times). **(G)** Photomicrograph of gastric antral biopsy showing abundant infiltrate of eosinophils (arrows) amongst lymphocytes and plasma cells (H&E stain; original magnification, 40 \times). **(H and I)** Endoscopic images showing (H) furrowing and (I) trachealization in the middle esophagus, suggestive of eosinophilic esophagitis.

80 uniquely increased hits, which did not overlap with WT nor with each other (Fig. 3 H, Fig. S3 F, and Table S6). This suggests that the altered activity of both p.E382Q and p.D419G is not restricted to enhanced activity of known STAT6 targets alone. Further investigation through gene set enrichment analyses (GSEA) showed increased enrichment in IL-4-STAT6 target genes at baseline (Fig. 3 I and Table S7), increased enrichment in T helper 2 (T_H2) drivers after stimulation (Elo et al., 2010; Fig. 3 J and Table S7), and increased enrichment in proliferation pathways for p.D419G consistent with its known oncogenic activity (Ritz et al., 2009; Tate et al., 2019; Yildiz et al., 2015; Fig. S3 G).

Patients with GOF STAT6 variants have slower STAT6 dephosphorylation kinetics after IL-4 stimulation and an enhanced T_H2 signature

To further investigate the role of STAT6 GOF variants in primary cells, STAT6 phosphorylation was quantified in patient samples. Unexpectedly, we found no differences in the percentage of phospho-STAT6 positive cells between patients and healthy controls after IL-4 stimulation over a 60 min time course nor after stimulation with different doses of IL-4 (Fig. S4, A and B). However, differences emerged when we monitored the kinetics of STAT6 dephosphorylation after stimulation (Fig. 4, A and B; and Fig. S4 C). Specifically, washing out of IL-4 led to slower dephosphorylation kinetics of STAT6 in most patient cells compared to healthy controls (Fig. 4, A and B; and Fig. S4 D), supporting a GOF mechanism in patient lymphocytes. We did note that one of our kindreds did not display delayed dephosphorylation (Fig. S4 D), suggesting that this might not be the only GOF mechanism. Indeed, increased STAT6 activity without phosphorylation has previously been reported in follicular lymphoma research studying the p.D419 mutational hotspot (Yildiz et al., 2015).

Given that the STAT6 axis is critical for the differentiation of T_H2 cells (Kaplan et al., 1996), a subset of $CD4^+$ helper T cells that is a major contributor to the pathogenesis of allergic disease, we next investigated T_H2 signatures in these patients. Patients showed skewing towards T_H2 pathway activity compared to healthy controls based on higher levels of the T_H2 cytokines IL-5, IL-13, and IL-4 as measured by flow cytometry (Fig. 4, C and D), or through transcriptomic signature by single-cell RNA sequencing (scRNAseq; Fig. 4 E). High throughput proteomics also validated the increased IL-4 expression, but not high IL-13 expression (Fig. S4 E). Differences in proportions of other subsets of helper T cells were restricted to higher IL-21 $^+$ cells in patient memory $CD4^+$ T cells (Fig. S4 F). scRNAseq showed that patient B cells expressed high *IGHE* and low *IGHG3* (Fig. 4 F), reflecting patterns opposite of those seen in STAT6 knockout mice (Shimoda et al., 1996;

Sulczewski et al., 2021), and $CD4^+$ T cells express high *GATA3*. scRNAseq further demonstrated that *IL4R*, a gene encoding a key receptor that mediates STAT6 activation, was upregulated in all B and T cell subsets (Fig. 4 F and Fig. S4 G).

Using flow cytometry, we confirmed that IL-4R α expression was significantly higher on both naive and memory $CD4^+$ T cells of seven patients from three different kindreds compared to nine healthy controls (Fig. 5 A). IL-4R α expression was also found to be higher in non-class switched memory and class switched memory B cells of unstimulated patient primary cells (Fig. 5 B). These findings suggest higher baseline activity of STAT6 in patient cells driving IL-4R α expression similar to that seen in our Jurkat model (Fig. 3, G–J; and Tables S6 and S7). Finally, we measured the expression of CD23 (the low-affinity IgE receptor, Fc ϵ RII) which is known to be upregulated by STAT6 (Fig. S3 B; Kneitz et al., 2000) and we found higher expression of CD23 on all subsets of patient B cells at baseline (Fig. 5 B) and following stimulation with IL-4 (Fig. S4 H). Taken together, these experiments conducted using primary patient cells further confirm the STAT6 GOF phenotype.

JAK inhibitors and IL-4R α monoclonal antibody can be used as potential therapeutics for patients with STAT6 GOF variants

Due to the severity of the multi-system allergic disease experienced by the patients in our cohort, various treatment approaches were used over the years. Corticosteroids, administered topically and systemically, were the mainstay of treatment for most patients. Unfortunately, even high doses of corticosteroids were unable to control the allergic inflammation and they were responsible for many side-effects including cataracts and osteoporosis. Other treatments used in this cohort that proved ineffective included topical tacrolimus, oral methotrexate, and mepolizumab (an anti-IL-5 monoclonal antibody).

Having demonstrated that heterozygous *STAT6* variants lead to higher STAT6 activity and T_H2 immunological skewing, we tested in vitro whether targeting the STAT6 pathway could be clinically beneficial. Based on our findings of higher phosphorylation of STAT6, and higher expression of IL-4R α , we selected the JAK inhibitors, ruxolitinib and tofacitinib, and the anti-IL-4R α antibody, dupilumab, as drugs to test in vitro as they are all used clinically for treatment of allergic disease (Bacharier et al., 2021; Beck et al., 2014; Bissonnette et al., 2016; Kim et al., 2020). We demonstrated that both ruxolitinib and tofacitinib effectively decreased the patient-specific enhanced STAT6 phosphorylation/activation in HEK293 cells at baseline and after IL-4 stimulation, whereas dupilumab inhibited IL-4 mediated increase in STAT6 activity (Fig. 6 A and Fig. S5 A). We further confirmed in

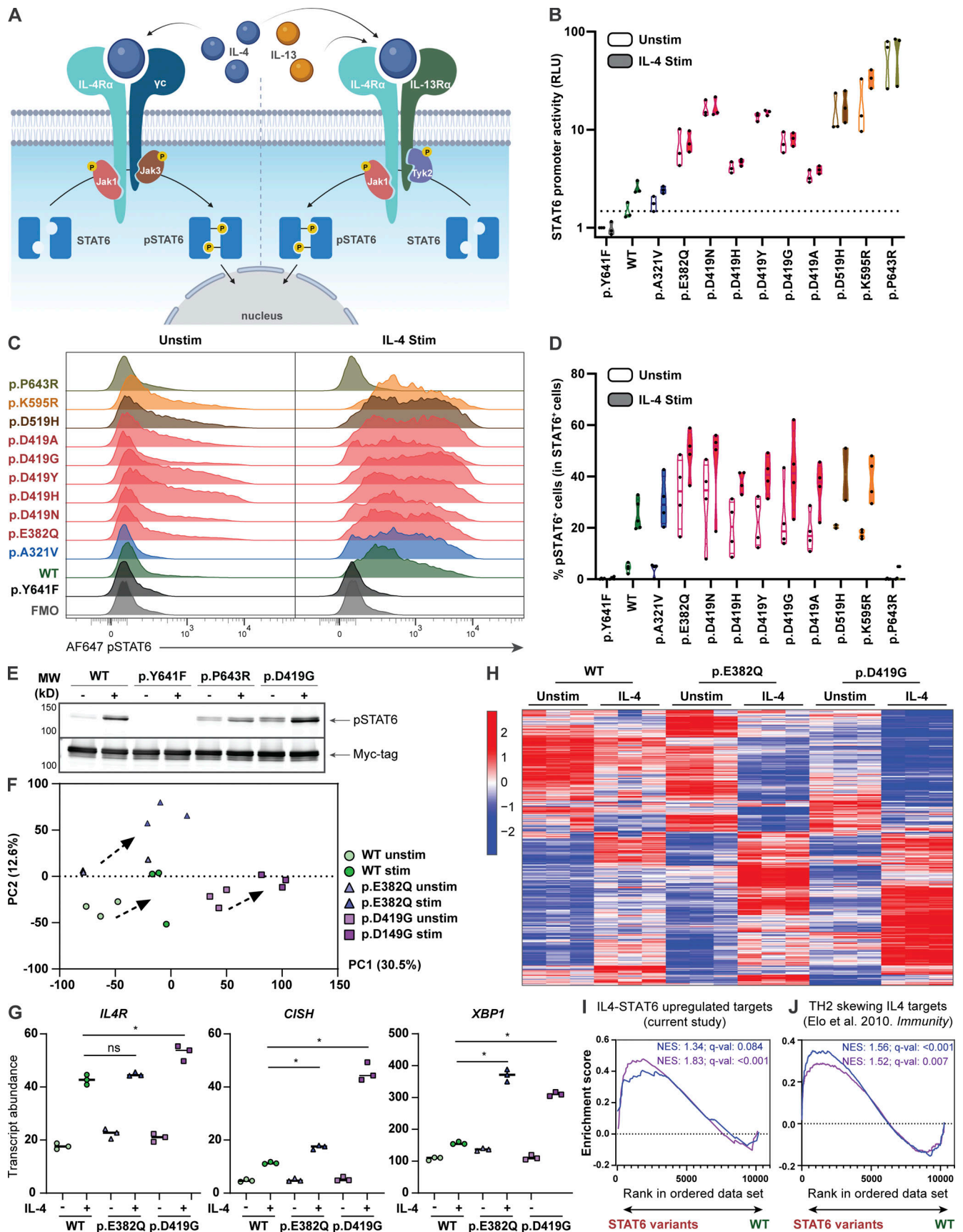


Figure 3. **STAT6** variants lead to increased **STAT6** activity in HEK293 cells and Jurkat T cells. **(A)** Schematic illustrating classical IL-4-mediated **STAT6** activation, dimerization, and phosphorylation. **(B)** Luciferase assay of **STAT6** activity on a plasmid containing a 4 \times **STAT6** binding site (TTCCCAAGAA; the

underlined bases represent two half-sites for STAT6-specific binding) for WT-, different STAT6 variant-transfected HEK293 cells before and after stimulation with IL-4 (0.02 ng/ml for 4 h); $n = 3$. **(C)** Phospho-STAT6 (Y641) expression in WT- and STAT6 variant-transfected HEK293 cells before and after treatment with IL-4 (10 ng/ml for 30 min). Gating strategy for pSTAT6⁺ cells can be found in Fig. S3 C. **(D)** Quantification of C; $n = 4$. **(E)** Immunoblot in HEK293 cells transfected with WT-, inactive- (p.Y641F), p.P643R-, and p.D419G-STAT6 variants for pSTAT6, and Myc-tag before and after treatment with IL-4 (10 ng/ml for 30 min); $n = 3$. Full-length immunoblot for this can be found in Fig. S3, D and E. **(F)** Principal component analysis (PCA) comparing unstimulated and stimulated (100 ng/ml IL-4 for 4 h) WT (green), p.E382Q (blue), and p.D419G (purple) STAT6-transduced Jurkat T cells. Individual symbols represent technical replicates of one transduced pool for each genotype. PC1 and PC2 contribution is shown in brackets. **(G)** Normalized counts comparing stimulated WT (green) vs. p.E382Q (blue) or p.D419G (purple), for *IL4R*, *CISH*, and *XBPI*. **(H)** Heatmap representation of normalized counts of a transcription set defined as IL-4 targets in transduced Jurkat T cells. **(I and J)** Asterisk indicates adjusted P value <0.05. GSEA plots for (I) curated STAT6 target genes comparing WT vs. either p.E382Q (blue) or p.D419G (purple) at baseline, or (J) IL-4-T_H2 targets genes comparing WT vs. either p.E382Q (blue) or p.D419G (purple) after stimulation with IL-4. Normalized enrichment score and adjusted P value are shown. Source data are available for this figure: SourceData F3.

patient primary cells that tofacitinib accelerated STAT6 dephosphorylation following IL-4 stimulation (Fig. 6 B). These data suggest the potential clinical benefit of directly targeting the IL-4/STAT6 pathway in patients with STAT6 GOF variants.

Once their STAT6 GOF variant was identified, three of the patients were started on dupilumab and all showed significant clinical improvement. P6, who has been on treatment with dupilumab for over 2 yr, serves as an illustrative example. Mirroring peripheral blood eosinophil counts (Fig. S5 B), repeated whole blood RNAseq showed global transcriptomic changes that were suggestive of mildly increased eosinophilic and allergic gene signatures after 38 d, followed by a shift of the transcriptome towards healthy controls after 123 and 492 d, respectively (Fig. 6 C and Fig. S5, C–E). scRNAseq confirmed a decrease in T_H2 gene signatures 2 yr following initiation of dupilumab, accompanied by a decrease in the expression of IL-4R on both naive CD4⁺ and CD8⁺ T cells (Fig. 6, D–E). Clinically, these changes were accompanied by dramatic increase in growth velocity, improved skin condition as quantified by SCORAD (SCORing atopic dermatitis) and EASI (eczema area and severity index) scores, and the ability to wean from oral corticosteroids (Fig. 6, F–H). Similarly, P1 experienced remarkable clinical benefits with dupilumab with improved skin inflammation (Fig. 6 D), resolution of pruritus, and the ability to discontinue oral daily high dose corticosteroids. In addition to resolution of skin inflammation with dupilumab, P2 was able to discontinue swallowed budesonide without a flare in the severity of her eosinophilic esophagitis. Our preclinical data also suggested that JAK inhibitors may be beneficial (Fig. 6, A and B), and P4 had received tofacitinib (5 mg/d) for 2 mo at the time this manuscript was finalized. His initial response to tofacitinib was encouraging with less dysphagia, less esophageal food impaction, improved endoscopic appearance of the esophagus, and a marked reduction in the number of intraepithelial eosinophils.

Discussion

We present a combination of clinical, genetic, molecular, and transcriptional evidence of a new human disorder caused by germline AD GOF STAT6 variants in 16 patients with life-long severe allergic disease. These variants led to sustained STAT6 phosphorylation, increased STAT6 target gene expression, and T_H2 skewed transcriptional profile. Importantly, we demonstrate in three patients that dupilumab treatment is a highly effective

targeted therapeutic option, improving both clinical manifestations of disease and immunological biomarkers.

Although the full phenotype(s) of individuals with GOF STAT6 variants will only be uncovered through the identification of additional affected individuals, we propose to classify human germline AD GOF STAT6 syndrome as a PAD (Lyons and Milner, 2018; Milner, 2020; Vaseghi-Shanjani et al., 2021). Based on our study, possible clinical “red flags” for this new disorder include: (i) early life onset; (ii) peripheral blood eosinophilia; (iii) elevated serum IgE; (iii) widespread, treatment-resistant atopic dermatitis; (iv) multiple food and drug allergies; (v) severe (and even fatal) anaphylaxis; (vi) recurrent skin and respiratory infections; (vii) eosinophilic gastrointestinal disorder, including eosinophilic esophagitis; (viii) asthma; (ix) allergic rhinoconjunctivitis; (x) short stature; and possibly (xi) vascular malformations of the brain.

STAT6 is intimately linked to the biology of allergic inflammation. The central and most studied role of STAT6 is in mediating the biological effects of IL-4, a cytokine necessary for T_H2 differentiation, B cell survival, proliferation, and class switching to IgE (Elo et al., 2010; Takeda et al., 1996), as well as in driving M2 macrophage polarization (Ginhoux et al., 2016). In T cells, STAT6 activation induces the expression of GATA3, the master regulator of T_H2 differentiation, which in turn enhances expression of IL-4, IL-5, and IL-13, cytokines necessary for promoting allergic responses by activating mast cells and eosinophils (Sloka et al., 2011). The presence of greater T_H2 cell populations, or T_H2 cells producing copious amounts of IL-4/IL-5/IL-13, could be a driver of the observed allergic phenotype presented in our patients. Elevated IgE in partnership with mast cells is important for both acute and chronic manifestations of allergic disorders and can be an additional driver of the allergic diathesis (Galli and Tsai, 2012). STAT6 hyperactivation in airway epithelial cells and resident dendritic cells can further create an environment favoring asthma and chronic lung disease, as this would induce production of chemokines that promote T_H2 cells and eosinophil recruitment (Matsukura et al., 2001; Medoff et al., 2009). Population genetics provide further support for the central role that STAT6 plays in the development of human allergic disease. Multiple independent genome-wide association studies (GWAS) have found that polymorphisms in STAT6 associate with many allergic conditions (Table 1). Our study expands this appreciation of the role of STAT6 in human disease by establishing that heterozygous GOF variants cause a monogenic form of severe allergic disease.

IL13⁺, and IL4⁺ cells in memory CD4⁺ T cells of one representative patient, along with one representative healthy control. **(D)** Quantification of C showing IL5⁺, IL13⁺, and IL4⁺ cells in patients along with 15 age-matched healthy controls. **, P < 0.01; ***, P < 0.001. **(E)** Uniform manifold approximation and projection (UMAP) visualization of scRNAseq done on enriched T cells comparing one patient with one age-matched healthy control. **(F)** Dot plot showing expression of selected differentially expressed genes (adjusted P value < 0.05) observed in scRNAseq between patient and healthy control and associated with T cells, B cells, monocytes, or dendritic cells.

The fatal cerebral aneurysm in P10 (p.E382Q) was not clinically anticipated, but it is possible that the *STAT6* GOF variant also increased the risk of developing cerebral aneurysms. Indeed, P1 (p.D419G) also had multiple rare anatomical variants in the arteries of the Circle of Willis. Intracranial aneurysms have been reported in patients with both *STAT3* loss-of-function (LOF) and *STAT1* GOF (Chandesris et al., 2012; Dadak et al., 2017; Toubiana et al., 2016). Increased activation of other *STAT* family members, including *STAT2*, *STAT3*, and *STAT5* have also been observed in human abdominal aortic aneurysms (*STAT6* was not evaluated), although it is not clear whether enhanced *STAT* phosphorylation contributes to aneurysms or is the result of inflammation caused by aneurysms (Liao et al., 2012). As more individuals with *STAT6* GOF variants are identified, the possibility of cerebral vascular anomalies warrants investigation.

It is noteworthy that the oldest patient in this cohort, P7 (p.D419H), experienced recurrent B cell lymphoma—follicular lymphoma at 49 yr and diffuse large B cell lymphoma at age 60 yr. Activating somatic mutations in *STAT6* are well documented in B cell lymphoma with amino acid D419 being a particular mutational hotspot (Ritz et al., 2009; Tate et al., 2019; Yildiz et al., 2015). The patient's p.D419H variant has been reported multiple times as a somatic mutation in COSMIC, as have other variants found in our patient cohort (i.e., p.D419, p.D519, and p.P643). More patients will need to be identified and followed to fully define the phenotype caused by germline *STAT6* GOF variants, but it is biologically plausible that these patients may be at higher risk of developing B cell malignancies warranting enhanced clinical vigilance.

A GOF *STAT6* model (designated *STAT6VT*) has previously been described in vitro (Daniel et al., 2000) and has been used to study chronic atopic dermatitis in mouse models (Bruns et al., 2003; DaSilva-Arnold et al., 2018). *STAT6VT* has the substitution of two amino acid residues, at positions 547 and 548, in the SH2 domain resulting in a *STAT6* mutant that is constitutively active in an IL-4-independent manner and is unresponsive to IL-4 stimulation (Daniel et al., 2000). The humans we identified with *STAT6* GOF variants and *STAT6VT* mice share a number of key features of the allergic diathesis, including elevated serum IgE and chronic atopic dermatitis. Very recently, a report was published describing a father and his two sons with severe allergic disease who were all heterozygous for the GOF *STAT6* variant p.E377K (Suratannon et al., 2022). This new family shares many of the features we report in our cohort of 10 families (Fig. 2 A), further emphasizing that patients with early onset severe allergic disease should be assessed for underlying monogenic gene defects, including *STAT6*.

There is now a growing list of human single gene defects that cause the classic hyper-IgE phenotypic triad of eczema,

recurrent skin and lung infections, and elevated serum IgE (Freeman and Milner, 2020; Vaseghi-Shanjani et al., 2021; Zhang et al., 2018). AD hyper-IgE syndrome caused by dominant negative variants in *STAT3* (i.e., Job's syndrome or *STAT3* LOF) is the best characterized of these conditions, but this list of disorders also includes other AD (*IL6ST*; Beziat et al., 2020) and autosomal recessive (AR; *ZNF341* [Béziat et al., 2018], *IL6ST* [Shahin et al., 2019]) disorders (Bergerson and Freeman, 2019; Minegishi, 2021). Notably, the patients we identified with *STAT6* GOF variants did exhibit some of the extra-immunological features typical of *STAT3* LOF, specifically hyperextensible joints, pathologic fractures, and vascular anomalies (Bergerson and Freeman, 2019).

Beyond defining the phenotype of *STAT6* GOF, we also present laboratory and clinical evidence supporting the effectiveness of dupilumab and tofacitinib treatment in these patients. It was notable that the three patients (P1, P2, and P6) who received dupilumab have experienced dramatic improved atopic dermatitis and could be weaned off systemic corticosteroids. P6, who had short stature and delayed bone age before starting the biologic agent, experienced rapid height and weight gain following initiation of dupilumab. In addition to the documented clinical benefits of dupilumab therapy in patients with *STAT6* GOF, we also present early data suggesting that the JAK inhibitors, ruxolitinib or tofacitinib, may be effective in this patient population.

While this study has many strengths, notably the extreme allergic phenotype of the 16 patients combined with in-depth functional assessment of their *STAT6* variants; because of the global nature of our cohort, the study does have limitations. First, patients were identified by their local expert clinicians as candidates for genetic assessment based on their extreme allergic phenotype and, in some cases, their family history. As a result, we do not have prospectively defined inclusion criteria. Second, the global nature of the cohort and variation in local access to medications such as dupilumab limited our ability to run the same assays on pre-treatment primary cells from all patients. Despite these limitations, our study does identify GOF variants in *STAT6* as a novel monogenic allergic disorder. We also present clinical and single cell evidence of the effectiveness of dupilumab in *STAT6* GOF patients. We anticipate that this discovery will facilitate the recognition and targeted treatment of more affected individuals and, with time, a full definition of the human genotype-phenotype relationship caused by germline human *STAT6* GOF variants will emerge, including understanding the risk of lymphoma.

Based on our findings reported in this study, we suggest that heterozygous GOF variants in *STAT6* be added to the list of AD causes of the hyper-IgE phenotype. While each of the conditions known to cause a hyper-IgE phenotype has some specific clinical

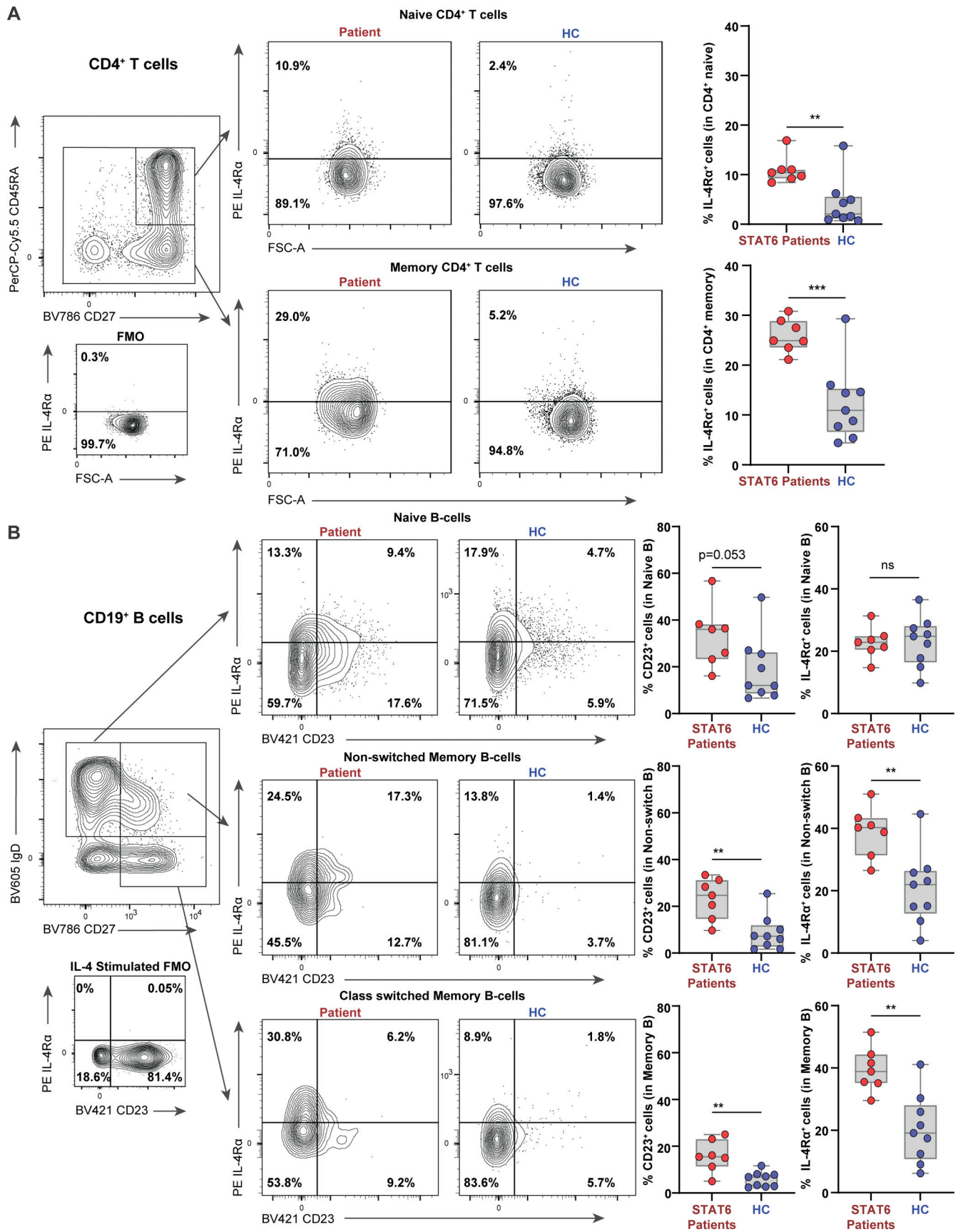


Figure 5. **Primary lymphocytes of STAT6 GOF patients display high expression of STAT6 target genes.** (A) Expression of IL4R α in naive and memory CD4⁺ cells is quantified as % positive cells in primary patient cells ($n = 7$, red) and healthy controls ($n = 9$, blue). Gating strategy for naive and memory and CD4⁺

is presented along with a dot plot for a fluorescence minus one (FMO) IL-4Ra sample to display IL-4Ra⁺ gating, as well as a representative dot plot for a patient and healthy control. **(B)** Expression of CD23 and IL4Ra in naive, non-class switched memory and memory B cells is quantified as % positive cells in primary patient cells ($n = 7$, red) and healthy controls ($n = 9$, blue). Gating strategy for B cell subsets is presented along with a dot plot for an FMO IL-4Ra sample to display IL-4Ra⁺ gating, as well as a representative dot plot for a patient and healthy control. Unpaired t test. **, $P < 0.01$; ***, $P < 0.001$.

features (e.g., viral skin infections are a defining feature of DOCK8 deficiency; Biggs et al., 2017; Chu et al., 2012), there is considerable clinical overlap and clinically approved testing of these pathways is rarely available. Therefore, we recommend genetic testing as the most efficient initial diagnostic approach to patients who experience severe allergic disease beginning very early in life. Finally, we demonstrate that dupilumab and JAK inhibition may be an effective targeted treatment options for patients with GOF *STAT6* variants.

Materials and methods

Ethical considerations

All procedures performed in the study were in accordance with the ethical standards of the institutional research committee and with the 1964 Helsinki declaration and its later amendments or comparable ethical standards. All study participants and/or their parents/guardians provided written informed consent. Research study protocols were approved by local institutions, specifically: The University of British Columbia Clinical Research Ethics Board (H09-01228, H15-00641), University College London Research Ethics Committee (04/Q0501/119, 06/Q0508/16), University of Hong Kong Institutional Review Board (UW 08-301), National Institutes of Health Institutional Review Board (NCT01164241), Children's Hospital of Philadelphia Institutional Review Board (19-016617), Children's Hospital Bambino Gesù Ethical Committee (1702_OPBG_2018).

Identification of *STAT6* variant via next-generation sequencing

Based on local availability, research or clinical next-generation sequencing of the genomic DNA was performed using either whole exome or a targeted panel approach (as described previously; Béziat et al., 2021; Campbell et al., 2022; Chovanec et al., 2022; Hebert et al., 2022; Murrell et al., 2022; Tarailo-Graovac et al., 2016). After bioinformatic analysis, de novo and inherited *STAT6* variants that were predicted to be damaging and that segregated with disease were identified in each family (Tables S4 and S5).

Generation and expression of *STAT6* variant plasmids

STAT6 variants described in this study were generated through site-directed mutagenesis (SDM) for transfection purposes. Expression of WT *STAT6* or *STAT6* variants were induced transiently in HEK293 cells using lipofectamine, or stably in Jurkat T cells using a lenti-viral approach. See supplemental methods at the end of the PDF for details.

Luciferase reporter assays

Luciferase reporter plasmids encoding a 4× *STAT6* binding site (TTCCCAAGAA; the underlined bases represent the two half-sites for *STAT6*-specific binding), encoding the promoter site for *CCL26*, and encoding the promoter site for *FCER2* were used to assess WT and variant *STAT6* promoter activity (Li et al., 2016; Yildiz et al., 2015). See supplemental methods at the end of the PDF for details.

Table 1. Number of published GWAS studies linking polymorphisms (SNPs) in *STAT6* to common allergic diseases in the population

Phenotype	Number of published associations	References
Asthma ^a	14	Daya et al., 2019; Demenais et al., 2018; Ferreira et al., 2019; Han et al., 2020; Johansson et al., 2019; Olafsdottir et al., 2020; Pickrell et al., 2016; Pividori et al., 2019; Sakaue et al., 2021; Shrine et al., 2019; Valette et al., 2021; Zhu et al., 2020; Zhu et al., 2018; Zhu et al., 2019
Eosinophil count	7	Astle et al., 2016; Chen et al., 2020; Höglund et al., 2022; Kachuri et al., 2021; Kichaev et al., 2019; Sakaue et al., 2021; Vuckovic et al., 2020
Allergic disease	3	Ferreira et al., 2017; Ferreira et al., 2020; Zhu et al., 2018
Atopic dermatitis/eczema	3	Johansson et al., 2019; Kichaev et al., 2019; Tanaka et al., 2021
Serum IgE level	2	Daya et al., 2021; Granada et al., 2012
Allergic sensitization	2	Bønnelykke et al., 2013; Waage et al., 2018
Allergic rhinitis	1	Johansson et al., 2019
Eosinophilic gastrointestinal disorders	1	Sleiman et al., 2014

Significant genome-wide associations ($P < 5 \times 10^{-8}$) between *STAT6* SNPs and all relevant allergic traits were obtained through the National Human Genome Research Institute-European Bioinformatics Institute GWAS Catalog (<https://www.ebi.ac.uk/gwas/>).

^aIncludes asthma, childhood-onset asthma, adult-onset asthma, and atopic asthma.

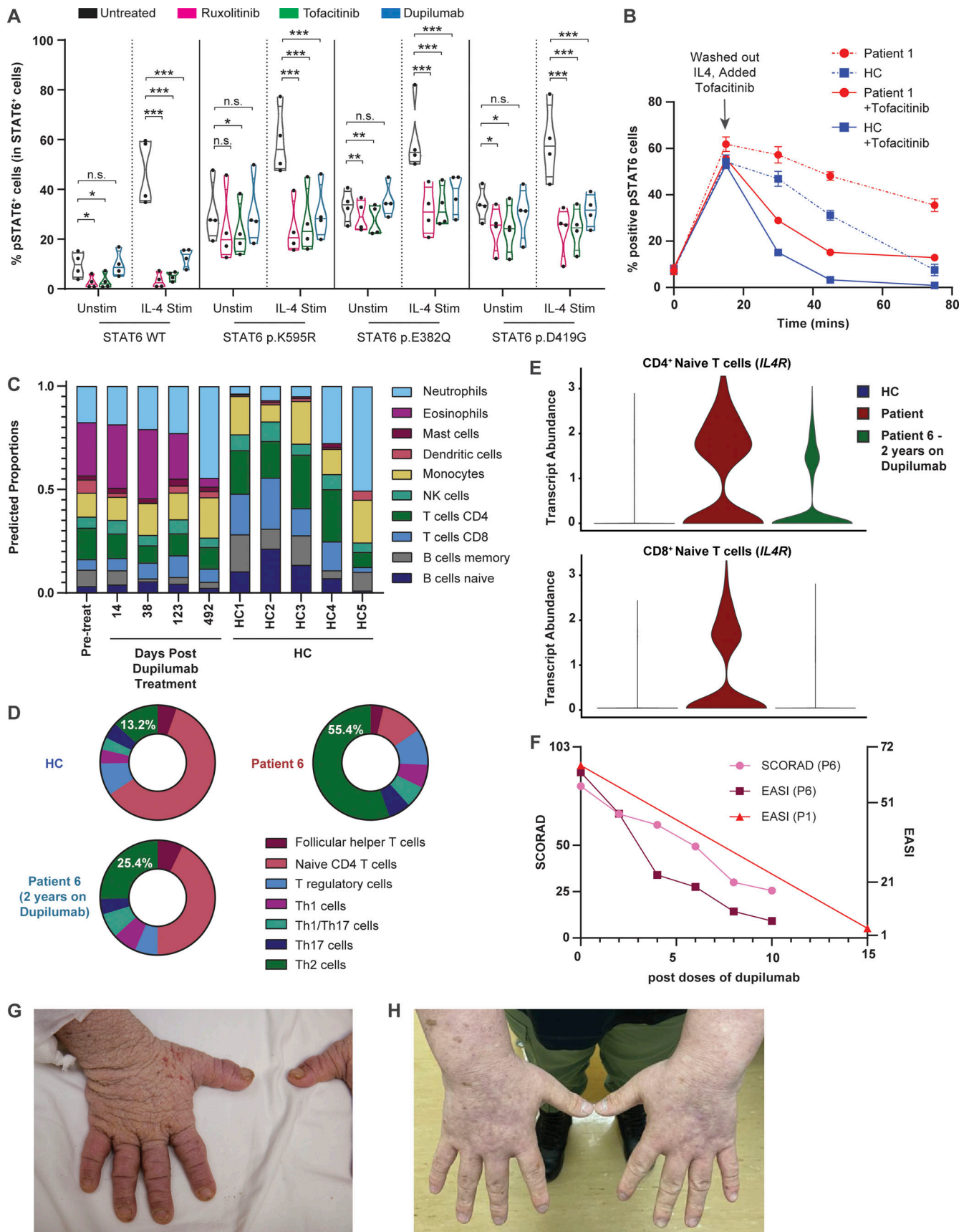


Figure 6. **JAK inhibitors and IL-4Ra antibody can be used as potential therapeutics for patients with GOF STAT6 variants.** (A) Quantification of phospho-STAT6 expression in transfected HEK293 cells left untreated (black) pre-treated with ruxolitinib (10 μ M, 1 h; pink), tofacitinib (10 μ M, 1 h; green), or

dupilumab (10 nM, 1 h; blue), before and after stimulation with IL-4 (10 ng/ml, 30 min). Individual points represent separate transfections for each genotype ($n = 4$). Gating strategy for pSTAT6⁺ cells can be found in Fig. S3 C. One-way ANOVA and Tukey's post-hoc test. *, $P < 0.05$; **, $P < 0.01$; ***, $P < 0.001$. (B) Quantification of pSTAT6⁺ cells in patient (red) and healthy control (blue) LCLs stimulated with IL-4 (10 ng/ml for 15 min), washed and incubated in tofacitinib (10 μ M) for 15, 30, and 60 min. Dotted translucent lines are indicative of no tofacitinib treatment (Fig. 4 B); $n = 1$. Gating strategy for pSTAT6⁺ cells can be found in Fig. S4 C. (C) Cell type proportion gene signature as determined by the software Cibersort, in a patient undergoing dupilumab treatment for 2 yr and five healthy controls. Cell labels are listed on the right. (D) Donut plot showing frequencies of CD4⁺ T helper subsets in one patient, an age-matched healthy control (Fig. 4 E), and a 2-yr post-dupilumab treatment patient sample as measured by scRNAseq on enriched T cells. Frequency of T_H2 cells is quantified in the donut plots of the different samples. (E) Violin plots showing expression of *IL4R* in the patient (red), healthy control (blue), and a 2-yr post-dupilumab sample (green). (F) Eczema scoring, EASI and SCORAD, for two patients after treatment with multiple doses of dupilumab. (G and H) Photographs of hands showing (G) the severity of atopic dermatitis before and (H) the improvement after dupilumab treatment.

Flow cytometry

(a) Phospho-flow cytometry: STAT6 phosphorylation was determined via phospho-flow cytometry for STAT6-transfected HEK293 cells, peripheral blood mononuclear cells (PBMCs), T cell blasts, and EBV-transformed lymphoblastoid B cell lines (LCLs). (b) Intracellular cytokine staining: Intracellular cytokine staining was conducted on nine patient PBMCs, alongside 15 healthy controls, to study CD4⁺ T helper subsets as previously described (Sharma et al., 2022). (c) CD23 and IL-4R α expression was studied on seven patient PBMCs and nine healthy control PBMCs. See supplemental methods at the end of the PDF for details.

Immunoblotting

Immunoblotting was conducted as previously described (Sharma et al., 2022) to assess the phosphorylation status of p.P643R STAT6 variant, as phosphorylation of this variant could not be detected via flow cytometry, using an antibody against the tyrosine 641 phosphorylation site. See supplemental methods at the end of the PDF for details.

RNAseq

(a) Jurkat cells: To model transcriptomics changes caused by STAT6 variants, Jurkat T cells were transduced with either c.1144G>C, p.E382Q, c.1256A>G, p.D419G, or WT STAT6. The cells were either left unstimulated or stimulated with 100 ng/ml of IL-4 for 4 h and subsequently used for RNA extraction and sequencing. (b) Whole blood: Bulk RNAseq was done on 10 samples: one patient sample before dupilumab treatment initiation, four patient samples after dupilumab treatment initiation, and five healthy controls. (c) scRNAseq: Performed on PBMCs and enriched T cells from the patient sample before and 2 yr after dupilumab treatment, along with one age-matched healthy control. See supplemental methods at the end of the PDF for details.

Histology

Formalin-fixed, paraffin-embedded gastric, duodenal, and skin tissue were sectioned and subjected to H&E staining.

Structural modeling

The effects of the STAT6 variants on the protein function and structure were analyzed using three-dimensional models. SWISS-MODEL (Waterhouse et al., 2018) was used to model the variants based on a template structure of the human STAT6 transcription factor solved as a homodimer and in complex with

DNA (PDB: 4Y5W, resolution: 3.1 Å, chains A, C, M, and N; Li et al., 2016). Structures were visualized with UCSF Chimera (Pettersen et al., 2004).

Online supplemental material

Clinical narratives for each patient are presented as Data S1. Fig. S1 is a detailed structural model showing the DNA and STAT6 variant interface. Fig. S2 shows complete blood count and the immunological workup of all the patients. Fig. S3 shows additional in vitro data confirming the GOF nature of the STAT6 variants. Further workup of the primary patient cells is shown in Fig. S4. Additional IL4R α antibody and JAK inhibitor treatment data of cells and patients is presented in Fig. S5. Table S1 lists primers used for site-directed mutagenesis. Table S2 lists antibodies used for phospho-flow on different immune subsets. Table S3 lists antibodies used for T_H phenotyping in patient PBMCs. Pathogenicity prediction of the variants are presented in Tables S4 and S5. Tables S6 and S7 are gene lists from GSEA analysis shown in Fig. 3. Supplemental methods are listed at the end of the PDF.

Acknowledgments

We thank the National Institute for Health and Care Research (NIHR) BioResource volunteers for their participation, and gratefully acknowledge NIHR BioResource centers, National Health Service Trusts, and staff for their contribution. A list of NIHR BioResource Rare Diseases Consortium members is available at the end of the PDF. We would also like to acknowledge the Biomedical Research Centre Sequencing Core for their assistance with RNAseq and processing. We acknowledge the extended clinical care team at the National Institute of Allergy and Infectious Diseases who helped in the care and evaluation of Patient 11. We also thank the extended clinical team at the Department of Paediatrics and Adolescent Medicine, Queen Mary Hospital, Hong Kong, China for providing expert care and support. We thank the Genomics Core of the Centre for Pan-orOmic Sciences of the University of Hong Kong for their professional performance of bulk and scRNAseq. Finally, we thank the patients and their families for their trust and support.

This work was supported by grants from the Canadian Institutes of Health Research (PJT 178054; S.E. Turvey), Genome British Columbia (SIP007; S.E. Turvey), and BC Children's Hospital Foundation. S.E. Turvey holds a Tier 1 Canada Research Chair in Pediatric Precision Health and the Aubrey J. Tingle Professor of Pediatric Immunology. M. Sharma was supported

by a CIHR Frederick Banting and Charles Best Canada Graduate Scholarships Doctoral Award and University of British Columbia Four Year Doctoral Fellowship (4YF). H.Y. Lu is supported by a Canada Graduate Scholarship, 4YF, Killam Doctoral Scholarship, Friedman Award for Scholars in Health, and a BC Children's Hospital Research Institute Graduate Studentship. M. Vaseghi-Shanjani is funded by the Vanier Canada Graduate Scholarship and 4YF. The work by J. Heimall was supported by the Elizabeth Paige Lavin Endowed Chair fund. This project has also been funded in part with federal funds from the Division of Intramural Research of the National Institute of Allergy and Infectious Diseases, National Institutes of Health. The content of this publication does not necessarily reflect the views or policies of the Department of Health and Human Services, nor does mention of trade names, commercial products, or organizations imply endorsement by the US Government. The Laboratory of Human Genetics of Infectious Diseases is supported by the Howard Hughes Medical Institute, the Rockefeller University, the St. Giles Foundation, the French National Research Agency (ANR) under the "Investments for the Future" program (ANR-10-IAHU-01), ANR CARMIL2 (ANR-21-CE15-0034), Instituts Thématiques Multiorganismes (ITMO) Cancer of Aviesan, and Institut National du Cancer (INCa) within the framework of the 2021-2030 Cancer Control Strategy (on funds administered by the Institut National de la Santé et de la Recherche Médicale), the Integrative Biology of Emerging Infectious Diseases Laboratory of Excellence (ANR-10-LABX-62-IBEID), the French Foundation for Medical Research (EQU201903007798), the Square Foundation, Institut National de la Santé et de la Recherche Médicale, and Paris University Cité. This work was also supported by Children's Hospital Bambino Gesù, where L. Pacillo and B. Rivalta were supported by 4-yr doctoral scholarships. C. Cifaldi and C. Cancrini were supported by the Italian Ministry of Health; C. Cifaldi was supported with a 5x1000 Children's Hospital post-doctoral scholarship, and C. Cancrini holds a Development of Innovative Diagnostic and Therapeutic Approaches for PID grant (Programma di rete, NET-2011-02350069) and Ricerca Corrente. Additionally, the optimization of the Olink platform was supported by the PENTA Foundation, funded through an independent grant by ViiV Healthcare UK, named EPIICAL. Y.L. Lau is supported by the Society for the Relief of Disabled Children, Jeffrey Modell Foundation, Doris Zimmern Endowed Professorship in Community Child Health, and Chung Ko Lee and Cheung Yuen Kan Education and Research Fund. D. Leung is supported by the Croucher Foundation. J.S.D. Rosa Duque is supported by a donation in memory of Dr. Ton Lung Quong and Reverend Marion Quong. Z. Liu, R. Liang, and X. Yang are supported by the Edward and Yolanda Wong Fund. The funders had no role in study design, data collection and analysis, decision to publish, or preparation of the manuscript.

Author contributions: Conceptualization, methodology, formal analysis, investigation, visualization, writing—original draft preparation, writing—review and editing: M. Sharma, D. Leung, M. Momenilandi, L.C.W. Jones, L. Pacillo, A.E. James, J.R. Murrell, S. Delafontaine, J. Maimaris, M. Vaseghi-Shanjani, K.L. Del Bel, and H.Y. Lu. Investigation, resources, writing—review and editing: G.T. Chua, S. Di Cesare, O. Fornes, Z. Liu, G. Di Matteo, M.P. Fu, D. Amodio, I.Y.S. Tam, G.S.W. Chan, A.A.

Sharma, J. Dalmann, R. van der Lee, G. Blanchard-Rohner, S. Lin, Q. Philippot, P.A. Richmond, J.J. Lee, A. Matthews, M. Seear, A.K. Turvey, R.L. Philips, T.F. Brown-Whitehorn, C.J. Gray, K. Izumi, J.R. Treat, K.H. Wood, J. Lack, A. Khleborodova, J.E. Niemela, X. Yang, R. Liang, L. Kui, C.S.M. Wong, G.W.K. Poon, A. Hoischen, C.I. van der Made, J. Yang, K.W. Chan, J.S.D. Rosa Duque, P.P.W. Lee, M.H.K. Ho, B.H.Y. Chung, H.T.M. Le, W. Yang, P. Rohani, A. Fouladvand, H. Rokni-Zadeh, M. Changi-Ashtiani, M. Miryounesi, A. Puel, M. Shahrooei, A. Finocchi, P. Rossi, B. Rivalta, C. Cifaldi, A. Novelli, C. Passarelli, S. Arasi, D. Bullens, K. Sauer, T. Claeys, C.M. Biggs, E.C. Morris, S.D. Rosenzweig, J.J. O'Shea, W.W. Wasserman, H.M. Bedford, C.D.M. van Karnebeek, and P. Palma. Conceptualization, methodology, investigation, validation, visualization, resources, funding acquisition, project administration, supervision, writing—original draft preparation, writing—review and editing: S.O. Burns, I. Meyts, J.-L. Casanova, J.J. Lyons, N. Parvaneh, A.T.V. Nguyen, C. Cancrini, J. Heimall, H. Ahmed, M.L. McKinnon, Y.L. Lau, V. Beziat, and S.E. Turvey.

Disclosures: S. Delafontaine is supported by the Personal Research Foundation Flanders grant 11F4421N. T.F. Brown-Whitehorn reported grants from DBV Technology, "other" from DBV Technology, and grants from Regeneron outside the submitted work. J.R. Treat reported personal fees from Sanofi/Regeneron outside the submitted work. D. Bullens reported grants from Research Foundation Flanders and Sanofi Genzyme outside the submitted work. E.C. Morris reported personal fees from Quell Therapeutics Limited outside the submitted work. J.J. O'Shea reported a patent for Janus kinase inhibitors with royalties paid (National Institutes of Health). P. Palma reported grants from the ViiV Foundation and Chiesi Foundation outside the submitted work. S.O. Burns has received grant support from CSL Behring and personal fees or travel expenses from CSL Behring, Baxalta US Inc, Glaxo Smith Kline, and Biotest. I. Meyts reported grants from CSLBehring (paid to institution) and "other" from Boehringer-Ingelheim SAB (paid to institution) outside the submitted work. J. Heimall reported grants from Regeneron, CSL Behring, Enzyvant, and ADMA; and personal fees from CSL Behring, UpToDate, Enzyvant, ADMA, and CIRM outside the submitted work. No other disclosures were reported.

Submitted: 14 October 2022

Revised: 12 December 2022

Accepted: 9 February 2023

References

- Adzhubei, I.A., S. Schmidt, L. Peshkin, V.E. Ramensky, A. Gerasimova, P. Bork, A.S. Kondrashov, and S.R. Sunyaev. 2010. A method and server for predicting damaging missense mutations. *Nat. Methods*. 7:248-249. <https://doi.org/10.1038/nmeth0410-248>
- Aran, D., A.P. Looney, L. Liu, E. Wu, V. Fong, A. Hsu, S. Chak, R.P. Naikawadi, P.J. Wolters, A.R. Abate, et al. 2019. Reference-based analysis of lung single-cell sequencing reveals a transitional profibrotic macrophage. *Nat. Immunol.* 20:163-172. <https://doi.org/10.1038/s41590-018-0276-y>
- Astle, W.J., H. Elding, T. Jiang, D. Allen, D. Ruklisa, A.L. Mann, D. Mead, H. Bouman, F. Riveros-Mckay, M.A. Kostadima, et al. 2016. The allelic

- landscape of human blood cell trait variation and links to common complex disease. *Cell*. 167:1415–1429.e19. <https://doi.org/10.1016/j.cell.2016.10.042>
- Bacharier, L.B., J.F. Maspero, C.H. Katelaris, A.G. Fiocchi, R. Gagnon, I. de Mir, N. Jain, L.D. Sher, X. Mao, and D. Liu, et al. 2021. Dupilumab in children with uncontrolled moderate-to-severe asthma. *N. Engl. J. Med.* 385: 2230–2240. <https://doi.org/10.1056/NEJMoa2106567>
- Beck, L.A., D. Thaçi, J.D. Hamilton, N.M. Graham, T. Bieber, R. Rocklin, J.E. Ming, H. Ren, R. Kao, E. Simpson, et al. 2014. Dupilumab treatment in adults with moderate-to-severe atopic dermatitis. *N. Engl. J. Med.* 371: 130–139. <https://doi.org/10.1056/NEJMoa1314768>
- Bergerson, J.R.E., and A.F. Freeman. 2019. An update on syndromes with a hyper-IgE phenotype. *Immunol. Allergy Clin. North Am.* 39:49–61. <https://doi.org/10.1016/j.iac.2018.08.007>
- Bettigole, S.E., R. Lis, S. Adoro, A.H. Lee, L.A. Spencer, P.F. Weller, and L.H. Glimcher. 2015. The transcription factor XBP1 is selectively required for eosinophil differentiation. *Nat. Immunol.* 16:829–837. <https://doi.org/10.1038/ni.3225>
- Béziat, V., J. Li, J.X. Lin, C.S. Ma, P. Li, A. Bousfiha, I. Pellier, S. Zoghi, S. Baris, S. Keles, et al. 2018. A recessive form of hyper-IgE syndrome by disruption of ZNF341-dependent STAT3 transcription and activity. *Sci. Immunol.* 3:3. <https://doi.org/10.1126/sciimmunol.aat4956>
- Béziat, V., F. Rapaport, J. Hu, M. Titeux, M. Bonnet des Claustres, M. Bourgey, H. Griffin, É. Bandet, C.S. Ma, R. Sherkat, et al. 2021. Humans with inherited T cell CD28 deficiency are susceptible to skin papillomaviruses but are otherwise healthy. *Cell*. 184:3812–3828.e30. <https://doi.org/10.1016/j.cell.2021.06.004>
- Beziat, V., S.J. Tavernier, Y.H. Chen, C.S. Ma, M. Materna, A. Laurence, J. Staal, D. Aschenbrenner, L. Roels, L. Worley, et al. 2020. Dominant-negative mutations in human IL6ST underlie hyper-IgE syndrome. *J. Exp. Med.* 217:e20191804. <https://doi.org/10.1084/jem.20191804>
- Biggs, C.M., S. Keles, and T.A. Chatila. 2017. DOCK8 deficiency: Insights into pathophysiology, clinical features and management. *Clin. Immunol.* 181: 75–82. <https://doi.org/10.1016/j.clim.2017.06.003>
- Bissonnette, R., K.A. Papp, Y. Poulin, M. Gooderham, M. Raman, L. Mallbris, C. Wang, V. Purohit, C. Mamolo, J. Papacharalambous, and W.C. Ports. 2016. Topical tofacitinib for atopic dermatitis: A phase IIa randomized trial. *Br. J. Dermatol.* 175:902–911. <https://doi.org/10.1111/bjd.14871>
- Bolton, S.M., A.F. Kagalwalla, and J.B. Wechsler. 2018. Eosinophilic esophagitis in children: Endoscopic findings at diagnosis and post-intervention. *Curr. Gastroenterol. Rep.* 20:4. <https://doi.org/10.1007/s11894-018-0607-z>
- Bønnelykke, K., M.C. Matheson, T.H. Pers, R. Granell, D.P. Strachan, A.C. Alves, A. Linneberg, J.A. Curtin, N.M. Warrington, and M. Standl, et al. 2013. Meta-analysis of genome-wide association studies identifies ten loci influencing allergic sensitization. *Nat. Genet.* 45:902–906. <https://doi.org/10.1038/ng.2694>
- Bruns, H.A., U. Schindler, and M.H. Kaplan. 2003. Expression of a constitutively active Stat6 in vivo alters lymphocyte homeostasis with distinct effects in T and B cells. *J. Immunol.* 170:3478–3487. <https://doi.org/10.4049/jimmunol.170.7.3478>
- Campbell, T.M., Z. Liu, Q. Zhang, M. Moncada-Velez, L.E. Covill, P. Zhang, I. Alavi Darazam, P. Bastard, L. Bizien, G. Bucciol, et al. 2022. Respiratory viral infections in otherwise healthy humans with inherited IRF7 deficiency. *J. Exp. Med.* 219:e20220202
- Chandesris, M.O., A. Azarine, K.T. Ong, S. Taleb, P. Boutouyrie, E. Mousseaux, M. Romain, E. Bozec, S. Laurent, N. Boddaert, et al. 2012. Frequent and widespread vascular abnormalities in human signal transducer and activator of transcription 3 deficiency. *Circ. Cardiovasc. Genet.* 5:25–34. <https://doi.org/10.1161/CIRCGENETICS.111.961235>
- Chen, M.-H., L.M. Raffield, A. Mousas, S. Sakaue, J.E. Huffman, A. Moscatti, B. Trivedi, T. Jiang, P. Akbari, and D. Vuckovic, et al. 2020. Trans-ethnic and ancestry-specific blood-cell genetics in 746,667 individuals from 5 global populations. *Cell*. 182:1198–1213.e14. <https://doi.org/10.1016/j.cell.2020.06.045>
- Chen, Y., A.T. Lun, and G.K. Smyth. 2016. From reads to genes to pathways: Differential expression analysis of RNA-seq experiments using rsubread and the edgeR quasi-likelihood pipeline. *F1000 Res.* 5:1438
- Chovanec, J., I. Tunc, J. Hughes, J. Halstead, A. Mateja, Y. Liu, M. O’Connell, J. Kim, Y.H. Park, Q. Wang, et al. 2022. Genetically determining individualized clinical reference ranges for the biomarker tryptase can limit unnecessary procedures and unmask myeloid neoplasms. *Blood Adv.*:bloodadvances.2022007936. <https://doi.org/10.1182/bloodadvances.2022007936>
- Chu, E.Y., A.F. Freeman, H. Jing, E.W. Cowen, J. Davis, H.C. Su, S.M. Holland, and M.L. Turner. 2012. Cutaneous manifestations of DOCK8 deficiency syndrome. *Arch. Dermatol.* 148:79–84. <https://doi.org/10.1001/archdermatol.2011.262>
- Dadak, M., R. Jacobs, J. Skuljec, A.C. Jirmo, Ö. Yildiz, F. Donnerstag, N.T. Baerlecken, R.E. Schmidt, H. Lanfermann, T. Skripuletz, et al. 2017. Gain-of-function STAT1 mutations are associated with intracranial aneurysms. *Clin. Immunol.* 178:79–85. <https://doi.org/10.1016/j.clim.2017.01.012>
- Daniel, C., A. Salvekar, and U. Schindler. 2000. A gain-of-function mutation in STAT6. *J. Biol. Chem.* 275:14255–14259. <https://doi.org/10.1074/jbc.C000129200>
- DaSilva-Arnold, S.C., A. Thyagarajan, L.J. Seymour, Q. Yi, J.R. Bradish, M. Al-Hassani, H. Zhou, N.J. Perdue, V. Nemeth, A. Krbanjevic, et al. 2018. Phenotypic acute and chronic atopic dermatitis-like lesions in Stat6^{VT} mice identifies a role for IL-33 in disease pathogenesis. *Arch. Dermatol. Res.* 310:197–207. <https://doi.org/10.1007/s00403-018-1807-y>
- Daya, M., C. Cox, N. Acevedo, M.P. Boorgula, M. Campbell, S. Chavan, M.H. Cho, G.L. David, P. Kachroo, and J. Lasky-Su, et al. 2021. Multiethnic genome-wide and HLA association study of total serum IgE level. *J. Allergy Clin. Immunol.* 148:1589–1595. <https://doi.org/10.1016/j.jaci.2021.09.011>
- Daya, M., N. Rafaels, T.M. Brunetti, S. Chavan, A.M. Levin, A. Shetty, C.R. Gignoux, M.P. Boorgula, G. Wojcik, and M. Campbell, et al. 2019. Association study in African-admixed populations across the Americas recapitulates asthma risk loci in non-African populations. *Nat. Commun.* 10:880. <https://doi.org/10.1038/s41467-019-08469-7>
- Demenaïs, F., P. Margaritte-Jeannin, K.C. Barnes, W.O.C. Cookson, J. Altmüller, W. Ang, R.G. Barr, T.H. Beaty, A.B. Becker, and J. Beilby, et al. 2018. Multiancestry association study identifies new asthma risk loci that colocalize with immune-cell enhancer marks. *Nat. Genet.* 50:42–53. <https://doi.org/10.1038/s41588-017-0014-7>
- Dierick, B.J.H., T. van der Molen, B.M.J. Flokstra-de Blok, A. Muraro, M.J. Postma, J.W.H. Kocks, and J.F.M. van Boven. 2020. Burden and socio-economics of asthma, allergic rhinitis, atopic dermatitis and food allergy. *Expert Rev. Pharmacoecon. Outcomes Res.* 20:437–453. <https://doi.org/10.1080/14737167.2020.1819793>
- Elo, L.L., H. Järvenpää, S. Tuomela, S. Raghav, H. Ahlfors, K. Laurila, B. Gupta, R.J. Lund, J. Tahvanainen, R.D. Hawkins, et al. 2010. Genome-wide profiling of interleukin-4 and STAT6 transcription factor regulation of human Th2 cell programming. *Immunity*. 32:852–862. <https://doi.org/10.1016/j.immuni.2010.06.011>
- Ferreira, M.A., J.M. Vonk, H. Baurecht, I. Marenholz, C. Tian, J.D. Hoffman, Q. Helmer, A. Tillander, V. Ullemer, and J. van Dongen, et al. 2017. Shared genetic origin of asthma, hay fever and eczema elucidates allergic disease biology. *Nat. Genet.* 49:1752–1757. <https://doi.org/10.1038/ng.3985>
- Ferreira, M.A.R., R. Mathur, J.M. Vonk, A. Szwajda, B. Brumpton, R. Granell, B.K. Brew, V. Ullemer, Y. Lu, and Y. Jiang, et al. 2019. Genetic architectures of childhood- and adult-onset asthma are partly distinct. *Am. J. Hum. Genet.* 104:665–684. <https://doi.org/10.1016/j.ajhg.2019.02.022>
- Ferreira, M.A.R., J.M. Vonk, H. Baurecht, I. Marenholz, C. Tian, J.D. Hoffman, Q. Helmer, A. Tillander, V. Ullemer, and Y. Lu, et al. 2020. Age-of-onset information helps identify 76 genetic variants associated with allergic disease. *PLoS Genet.* 16:e1008725. <https://doi.org/10.1371/journal.pgen.1008725>
- Freeman, A.F., and J.D. Milner. 2020. The child with elevated IgE and infection susceptibility. *Curr. Allergy Asthma Rep.* 20:65. <https://doi.org/10.1007/s11882-020-00964-y>
- Fung, S.Y., H.Y. Lu, M. Sharma, A.A. Sharma, A. Saferali, A. Jia, L. Abraham, T. Klein, M.R. Gold, L.D. Noterangelo, et al. 2021. MALT1-Dependent cleavage of HOIL1 modulates canonical NF- κ B signaling and inflammatory responsiveness. *Front. Immunol.* 12:749794. <https://doi.org/10.3389/fimmu.2021.749794>
- Galli, S.J., and M. Tsai. 2012. IgE and mast cells in allergic disease. *Nat. Med.* 18:693–704. <https://doi.org/10.1038/nm.2755>
- Ginhoux, F., J.L. Schultze, P.J. Murray, J. Ochando, and S.K. Biswas. 2016. New insights into the multidimensional concept of macrophage ontogeny, activation and function. *Nat. Immunol.* 17:34–40. <https://doi.org/10.1038/ni.3324>
- Goenka, S., and M.H. Kaplan. 2011. Transcriptional regulation by STAT6. *Immunol. Res.* 50:87–96. <https://doi.org/10.1007/s12026-011-8205-2>
- Gowthaman, U., J.S. Chen, B. Zhang, W.F. Flynn, Y. Lu, W. Song, J. Joseph, J.A. Gertie, L. Xu, M.A. Collet, et al. 2019. Identification of a T follicular

- helper cell subset that drives anaphylactic IgE. *Science*. 365:365. <https://doi.org/10.1126/science.aaw6433>
- Granada, M., J.B. Wilk, M. Tuzova, D.P. Strachan, S. Weidinger, E. Albrecht, C. Gieger, J. Heinrich, B.E. Himes, G.M. Hunninghake, et al. 2012. A genome-wide association study of plasma total IgE concentrations in the Framingham Heart Study. *J. Allergy Clin. Immunol.* 129:840–845.e21. <https://doi.org/10.1016/j.jaci.2011.09.029>
- Hafemeister, C., and R. Satija. 2019. Normalization and variance stabilization of single-cell RNA-seq data using regularized negative binomial regression. *Genome Biol.* 20:296. <https://doi.org/10.1186/s13059-019-1874-1>
- Han, Y., Q. Jia, P.S. Jahani, B.P. Hurrell, C. Pan, P. Huang, J. Gukasyan, N.C. Woodward, E. Eskin, F.D. Gilliland, et al. 2020. Genome-wide analysis highlights contribution of immune system pathways to the genetic architecture of asthma. *Nat. Commun.* 11:1776. <https://doi.org/10.1038/s41467-020-15649-3>
- Hebert, A., A. Simons, J.H.M. Schuurs-Hoeijmakers, H.J.P.M. Koenen, E. Zonneveld-Huijssoon, S.S.V. Henriët, E.J.H. Schatorjé, E.P.A.H. Hoppenreijns, E.K.S.M. Leenders, E.J.M. Janssen, et al. 2022. Trio-based whole exome sequencing in patients with suspected sporadic inborn errors of immunity: A retrospective cohort study. *Elife*. 11:e78469. <https://doi.org/10.7554/eLife.78469>
- Höglund, J., F. Hadizadeh, W.E. Ek, T. Karlsson, and Å. Johansson. 2022. Gene-based variant analysis of whole-exome sequencing in relation to eosinophil count. *Front. Immunol.* 13:862255. <https://doi.org/10.3389/fimmu.2022.862255>
- Johansson, Å., M. Rask-Andersen, T. Karlsson, and W.E. Ek. 2019. Genome-wide association analysis of 350 000 Caucasians from the UK Biobank identifies novel loci for asthma, hay fever and eczema. *Hum. Mol. Genet.* 28:4022–4041. <https://doi.org/10.1093/hmg/ddz175>
- Kachuri, L., S. Jeon, A.T. DeWan, C. Metayer, X. Ma, J.S. Witte, C.W.K. Chiang, J.L. Wiemels, and A.J. de Smith. 2021. Genetic determinants of blood-cell traits influence susceptibility to childhood acute lymphoblastic leukemia. *Am. J. Hum. Genet.* 108:1823–1835. <https://doi.org/10.1016/j.ajhg.2021.08.004>
- Kaplan, M.H., U. Schindler, S.T. Smiley, and M.J. Grusby. 1996. Stat6 is required for mediating responses to IL-4 and for development of Th2 cells. *Immunity*. 4:313–319. [https://doi.org/10.1016/S1074-7613\(00\)80439-2](https://doi.org/10.1016/S1074-7613(00)80439-2)
- Kichaev, G., G. Bhatia, P.-R. Loh, S. Gazal, K. Burch, M.K. Freund, A. Schoech, B. Pasaniuc, and A.L. Price. 2019. Leveraging polygenic functional enrichment to improve GWAS power. *Am. J. Hum. Genet.* 104:65–75. <https://doi.org/10.1016/j.ajhg.2018.11.008>
- Kim, B.S., M.D. Howell, K. Sun, K. Papp, A. Nasir, M.E. Kuligowski, I.S. Investigators, and INCB 18424-206 Study Investigators. 2020. Treatment of atopic dermatitis with ruxolitinib cream (JAK1/JAK2 inhibitor) or triamcinolone cream. *J. Allergy Clin. Immunol.* 145:572–582. <https://doi.org/10.1016/j.jaci.2019.08.042>
- Kim, Y., E.K. Kwon, J.H. Jeon, I. So, I.G. Kim, M.S. Choi, I.S. Kim, J.K. Choi, J.U. Jung, and N.H. Cho. 2012. Activation of the STAT6 transcription factor in Jurkat T-cells by the herpesvirus saimiri Tip protein. *J. Gen. Virol.* 93:330–340. <https://doi.org/10.1099/vir.0.036087-0>
- Kneitz, C., M. Goller, R. Seggewiss, A. Yaman, E. Serfling, and H.P. Tony. 2000. STAT6 and the regulation of CD23 expression in B-chronic lymphocytic leukemia. *Leuk. Res.* 24:331–337. [https://doi.org/10.1016/S0145-2126\(99\)00191-5](https://doi.org/10.1016/S0145-2126(99)00191-5)
- Kulpa, D.A., A. Talla, J.H. Brehm, S.P. Ribeiro, S. Yuan, A.G. Bebin-Blackwell, M. Miller, R. Barnard, S.G. Deeks, D. Hazuda, et al. 2019. Differentiation into an effector memory phenotype potentiates HIV-1 latency reversal in CD4⁺ T cells. *J. Virol.* 93:93. <https://doi.org/10.1128/JVI.00969-19>
- Kutner, R.H., X.Y. Zhang, and J. Reiser. 2009. Production, concentration and titration of pseudotyped HIV-1-based lentiviral vectors. *Nat. Protoc.* 4:495–505. <https://doi.org/10.1038/nprot.2009.22>
- Lemonnier, N., E. Melén, Y. Jiang, S. Joly, C. Ménard, D. Aguilar, E. Acosta-Perez, A. Bergström, N. Boutaoui, M. Bustamante, et al. 2020. A novel whole blood gene expression signature for asthma, dermatitis, and rhinitis multimorbidity in children and adolescents. *Allergy*. 75:3248–3260. <https://doi.org/10.1111/all.14314>
- Li, J., J.P. Rodriguez, F. Niu, M. Pu, J. Wang, L.W. Hung, Q. Shao, Y. Zhu, W. Ding, Y. Liu, et al. 2016. Structural basis for DNA recognition by STAT6. *Proc. Natl. Acad. Sci. USA*. 113:13015–13020. <https://doi.org/10.1073/pnas.1611228113>
- Liao, M., J. Xu, A.J. Clair, B. Ehrman, L.M. Graham, and M.J. Egleton. 2012. Local and systemic alterations in signal transducers and activators of transcription (STAT) associated with human abdominal aortic aneurysms. *J. Surg. Res.* 176:321–328. <https://doi.org/10.1016/j.jss.2011.05.041>
- Lu, H.Y., M. Sharma, A.A. Sharma, A. Lacson, A. Szpurko, J. Luiders, P. Dharmani-Khan, A. Shamel, P.A. Bell, G.M.T. Guilcher, et al. 2021. Mechanistic understanding of the combined immunodeficiency in complete human CARD11 deficiency. *J. Allergy Clin. Immunol.* 148:1559–1574.e13. <https://doi.org/10.1016/j.jaci.2021.04.006>
- Lundberg, M., A. Eriksson, B. Tran, E. Assarsson, and S. Fredriksson. 2011. Homogeneous antibody-based proximity extension assays provide sensitive and specific detection of low-abundant proteins in human blood. *Nucleic Acids Res.* 39:e102. <https://doi.org/10.1093/nar/gkr424>
- Lyons, J.J., and J.D. Milner. 2018. Primary atopic disorders. *J. Exp. Med.* 215:1009–1022. <https://doi.org/10.1084/jem.20172306>
- Matsukura, S., C. Stellato, S.N. Georas, V. Casolaro, J.R. Plitt, K. Miura, S. Kurosawa, U. Schindler, and R.P. Schleimer. 2001. Interleukin-13 up-regulates eotaxin expression in airway epithelial cells by a STAT6-dependent mechanism. *Am. J. Respir. Cell Mol. Biol.* 24:755–761. <https://doi.org/10.1165/ajrcmb.24.6.4351>
- Medoff, B.D., E. Seung, S. Hong, S.Y. Thomas, B.P. Sandall, J.S. Duffield, D.A. Kuperman, D.J. Erle, and A.D. Luster. 2009. CD11b⁺ myeloid cells are the key mediators of Th2 cell homing into the airway in allergic inflammation. *J. Immunol.* 182:623–635. <https://doi.org/10.4049/jimmunol.182.1.623>
- Mikita, T., D. Campbell, P. Wu, K. Williamson, and U. Schindler. 1996. Requirements for interleukin-4-induced gene expression and functional characterization of Stat6. *Mol. Cell. Biol.* 16:5811–5820. <https://doi.org/10.1128/MCB.16.10.5811>
- Milner, J.D. 2020. Primary atopic disorders. *Annu. Rev. Immunol.* 38:785–808. <https://doi.org/10.1146/annurev-immunol-042718-041553>
- Minegishi, Y. 2021. Hyper-IgE syndrome, 2021 update. *Allergol. Int.* 70:407–414. <https://doi.org/10.1016/j.alit.2021.07.007>
- Monaco, G., B. Lee, W. Xu, S. Mustafah, Y.Y. Hwang, C. Carre, N. Burdin, L. Visan, M. Ceccarelli, M. Poidinger, et al. 2019. RNA-seq signatures normalized by mRNA abundance allow absolute deconvolution of human immune cell types. *Cell Rep.* 26:1627–1640 e1627. <https://doi.org/10.1016/j.celrep.2019.01.041>
- Murrell, J.R., A.M.I. Nesbitt, S.W. Baker, K.B. Pechter, J. Balciuniene, X. Zhao, E.H. Denenberg, E.T. DeChene, C. Wu, P. Jayaraman, et al. 2022. Molecular diagnostic outcomes from 700 cases: What can we learn from a retrospective analysis of clinical exome sequencing? *J. Mol. Diagn.* 24:274–286. <https://doi.org/10.1016/j.jmoldx.2021.12.002>
- Newman, A.M., C.L. Liu, M.R. Green, A.J. Gentles, W. Feng, Y. Xu, C.D. Hoang, M. Diehn, and A.A. Alizadeh. 2015. Robust enumeration of cell subsets from tissue expression profiles. *Nat. Methods*. 12:453–457. <https://doi.org/10.1038/nmeth.3337>
- Novershtern, N., A. Subramanian, L.N. Lawton, R.H. Mak, W.N. Haining, M.E. McConkey, N. Habib, N. Yosef, C.Y. Chang, T. Shay, et al. 2011. Densely interconnected transcriptional circuits control cell states in human hematopoiesis. *Cell*. 144:296–309. <https://doi.org/10.1016/j.cell.2011.01.004>
- Olafsdottir, T.A., F. Theodors, K. Bjarnadottir, U.S. Bjornsdottir, A.B. Agustsdottir, O.A. Stefansson, E.V. Ivarsdottir, J.K. Sigurdsson, S. Benonisdottir, G.I. Eyjolfsson, et al. 2020. Eighty-eight variants highlight the role of T cell regulation and airway remodeling in asthma pathogenesis. *Nat. Commun.* 11:393. <https://doi.org/10.1038/s41467-019-14144-8>
- Pettersen, E.F., T.D. Goddard, C.C. Huang, G.S. Couch, D.M. Greenblatt, E.C. Meng, and T.E. Ferrin. 2004. UCSF Chimera—a visualization system for exploratory research and analysis. *J. Comput. Chem.* 25:1605–1612. <https://doi.org/10.1002/jcc.20084>
- Pickrell, J.K., T. Berisa, J.Z. Liu, L. Ségurel, J.Y. Tung, and D.A. Hinds. 2016. Detection and interpretation of shared genetic influences on 42 human traits. *Nat. Genet.* 48:709–717. <https://doi.org/10.1038/ng.3570>
- Pividori, M., N. Schoettler, D.L. Nicolae, C. Ober, and H.K. Im. 2019. Shared and distinct genetic risk factors for childhood-onset and adult-onset asthma: Genome-wide and transcriptome-wide studies. *Lancet Respir. Med.* 7:509–522. [https://doi.org/10.1016/S2213-2600\(19\)30055-4](https://doi.org/10.1016/S2213-2600(19)30055-4)
- Rapaport, F., B. Boisson, A. Gregor, V. Béziat, S. Boisson-Dupuis, J. Bustamante, E. Jouanguy, A. Puel, J. Rosain, Q. Zhang, et al. 2021. Negative selection on human genes underlying inborn errors depends on disease outcome and both the mode and mechanism of inheritance. *Proc. Natl. Acad. Sci. USA*. 118:118. <https://doi.org/10.1073/pnas.2001248118>
- Rentsch, P., M. Schubach, J. Shendure, and M. Kircher. 2021. CADD-Splice—improving genome-wide variant effect prediction using deep learning-derived splice scores. *Genome Med.* 13:31. <https://doi.org/10.1186/s13073-021-00835-9>

- Ritchie, M.E., B. Phipson, D. Wu, Y. Hu, C.W. Law, W. Shi, and G.K. Smyth. 2015. Limma powers differential expression analyses for RNA-sequencing and microarray studies. *Nucleic Acids Res.* 43:e47. <https://doi.org/10.1093/nar/gkv007>
- Ritz, O., C. Güter, F. Castellano, K. Dorsch, J. Melzner, J.P. Jais, G. Dubois, P. Gaulard, P. Möller, and K. Leroy. 2009. Recurrent mutations of the STAT6 DNA binding domain in primary mediastinal B-cell lymphoma. *Blood.* 114:1236–1242. <https://doi.org/10.1182/blood-2009-03-209759>
- Robinson, M.D., and G.K. Smyth. 2007. Moderated statistical tests for assessing differences in tag abundance. *Bioinformatics.* 23:2881–2887. <https://doi.org/10.1093/bioinformatics/btm453>
- Sakaue, S., M. Kanai, Y. Tanigawa, J. Karjalainen, M. Kurki, S. Koshiba, A. Narita, T. Konuma, K. Yamamoto, and M. Akiyama, et al. 2021. A cross-population atlas of genetic associations for 220 human phenotypes. *Nat. Genet.* 53:1415–1424. <https://doi.org/10.1038/s41588-021-00931-x>
- Shahin, T., D. Aschenbrenner, D. Cagdas, S.K. Bal, C.D. Conde, W. Garncarz, D. Medgyesi, T. Schwerdt, B. Karaatmaca, P.G. Cetinkaya, et al. 2019. Selective loss of function variants in cause Hyper-IgE syndrome with distinct impairments of T-cell phenotype and function. *Haematologica.* 104:609–621. <https://doi.org/10.3324/haematol.2018.194233>
- Sharma, M., M.P. Fu, H.Y. Lu, A.A. Sharma, B.P. Modi, C. Michalski, S. Lin, J. Dalmann, A. Salman, K.L. Del Bel, et al. 2022. Human complete NFAT1 deficiency causes a triad of joint contractures, osteochondromas, and B-cell malignancy. *Blood.* 140:1858–1874. <https://doi.org/10.1182/blood.2022015674>
- Shimoda, K., J. van Deursen, M.Y. Sangster, S.R. Sarawar, R.T. Carson, R.A. Tripp, C. Chu, F.W. Quelle, T. Nosaka, D.A. Vignali, et al. 1996. Lack of IL-4-induced Th2 response and IgE class switching in mice with disrupted Stat6 gene. *Nature.* 380:630–633. <https://doi.org/10.1038/380630a0>
- Shrine, N., M.A. Portelli, C. John, M. Soler Artigas, N. Bennett, R. Hall, J. Lewis, A.P. Henry, C.K. Billington, A. Ahmad, et al. 2019. Moderate-to-severe asthma in individuals of European ancestry: A genome-wide association study. *Lancet Respir. Med.* 7:20–34. [https://doi.org/10.1016/S2213-2600\(18\)30389-8](https://doi.org/10.1016/S2213-2600(18)30389-8)
- Sim, N.L., P. Kumar, J. Hu, S. Henikoff, G. Schneider, and P.C. Ng. 2012. SIFT web server: Predicting effects of amino acid substitutions on proteins. *Nucleic Acids Res.* 40:W452–W457. <https://doi.org/10.1093/nar/gks539>
- Sleiman, P.M.A., M.-L. Wang, A. Cianferoni, S. Aceves, N. Gonsalves, K. Nadeau, A.J. Bredenoord, G.T. Furuta, J.M. Spergel, and H. Hakonarson. 2014. GWAS identifies four novel eosinophilic esophagitis loci. *Nat. Commun.* 5:5593. <https://doi.org/10.1038/ncomms6593>
- Sloka, S., C. Silva, J. Wang, and V.W. Yong. 2011. Predominance of Th2 polarization by vitamin D through a STAT6-dependent mechanism. *J. Neuroinflammation.* 8:56. <https://doi.org/10.1186/1742-2094-8-56>
- Sulczewski, F.B., L.A. Martino, B. da Silva Almeida, M.M. Yamamoto, D.S. Rosa, and S.B. Boscardin. 2021. STAT6 signaling pathway controls germinal center responses promoted after antigen targeting to conventional type 2 dendritic cells. *Curr. Res. Immunol.* 2:120–131. <https://doi.org/10.1016/j.crimmu.2021.08.001>
- Suratannon, N., C. Ittiwut, W.A. Dik, R. Ittiwut, K. Meesilpavikkai, N. Isra-sena, P. Ingrungruanglert, V.A.S.H. Dalm, P.L.A. van Daele, A. Sanpavat, et al. 2022. A germline STAT6 gain-of-function variant is associated with early-onset allergies. *J. Allergy Clin. Immunol.* 151:565–571.e9
- Takeda, K., T. Tanaka, W. Shi, M. Matsumoto, M. Minami, S. Kashiwamura, K. Nakanishi, N. Yoshida, T. Kishimoto, and S. Akira. 1996. Essential role of Stat6 in IL-4 signalling. *Nature.* 380:627–630. <https://doi.org/10.1038/380627a0>
- Tanaka, N., M. Koido, A. Suzuki, N. Otomo, H. Suetsugu, Y. Kochi, K. Tomizuka, Y. Momozawa, Y. Kamatani, and S. Ikegawa, et al. 2021. Eight novel susceptibility loci and putative causal variants in atopic dermatitis. *J. Allergy Clin. Immunol.* 148:1293–1306. <https://doi.org/10.1016/j.jaci.2021.04.019>
- Tarailo-Graovac, M., C. Shyr, C.J. Ross, G.A. Horvath, R. Salvarinova, X.C. Ye, L.H. Zhang, A.P. Bhavsar, J.J. Lee, B.I. Drögemöller, et al. 2016. Exome sequencing and the management of neurometabolic disorders. *N. Engl. J. Med.* 374:2246–2255. <https://doi.org/10.1056/NEJMoal515792>
- Tate, J.G., S. Bamford, H.C. Jubb, Z. Sondka, D.M. Beare, N. Bindal, H. Boutselakis, C.G. Cole, C. Creatore, E. Dawson, et al. 2019. COSMIC: The Catalogue of somatic mutations in cancer. *Nucleic Acids Res.* 47: D941–D947. <https://doi.org/10.1093/nar/gky1015>
- Toubiana, J., S. Okada, J. Hiller, M. Oleastro, M. Lagos Gomez, J.C. Aldave Becerra, M. Ouachée-Chardin, F. Fouyssac, K.M. Girisha, and A. Etzioni, et al. 2016. Heterozygous STAT1 gain-of-function mutations underlie an unexpectedly broad clinical phenotype. *Blood.* 127:3154–3164. <https://doi.org/10.1182/blood-2015-11-679902>
- Valette, K., Z. Li, V. Bon-Baret, A. Chignon, J.-C. Bérubé, A. Eslami, J. Lamothe, N. Gaudreault, P. Joubert, M. Obeidat, et al. 2021. Prioritization of candidate causal genes for asthma in susceptibility loci derived from UK Biobank. *Commun. Biol.* 4:700. <https://doi.org/10.1038/s42003-021-02227-6>
- Vaseghi-Shanjani, M., K.L. Smith, R.J. Sara, B.P. Modi, A. Branch, M. Sharma, H.Y. Lu, E.L. James, K.J. Hildebrand, C.M. Biggs, and S.E. Turvey. 2021. Inborn errors of immunity manifesting as atopic disorders. *J. Allergy Clin. Immunol.* 148:1130–1139. <https://doi.org/10.1016/j.jaci.2021.08.008>
- Villarino, A.V., M. Gadina, J.J. O’Shea, and Y. Kanno. 2020. SnapShot: Jak-STAT signaling II. *Cell.* 181:1696–1696.e1691. <https://doi.org/10.1016/j.cell.2020.04.052>
- Villarino, A.V., Y. Kanno, and J.J. O’Shea. 2017. Mechanisms and consequences of Jak-STAT signaling in the immune system. *Nat. Immunol.* 18:374–384. <https://doi.org/10.1038/ni.3691>
- Vuckovic, D., E.L. Bao, P. Akbari, C.A. Lareau, A. Mousas, T. Jiang, M.-H. Chen, L.M. Raffield, M. Tardaguila, and J.E. Huffman, et al. 2020. The polygenic and monogenic basis of blood traits and diseases. *Cell.* 182: 1214–1231.e11. <https://doi.org/10.1016/j.cell.2020.08.008>
- Waage, J., M. Standl, J.A. Curtin, L.E. Jessen, J. Thorsen, C. Tian, N. Schoettler, C. Flores, A. Abdellaoui, and T.S. Ahluwalia, et al. 2018. Genome-wide association and HLA fine-mapping studies identify risk loci and genetic pathways underlying allergic rhinitis. *Nat. Genet.* 50:1072–1080. <https://doi.org/10.1038/s41588-018-0157-1>
- Waterhouse, A., M. Bertoni, S. Bienert, G. Studer, G. Tauriello, R. Gumienny, F.T. Heer, T.A.P. de Beer, C. Rempfer, L. Bordoli, et al. 2018. SWISS-MODEL: Homology modelling of protein structures and complexes. *Nucleic Acids Res.* 46:W296–W303. <https://doi.org/10.1093/nar/gky427>
- Wick, K.R., and M.T. Berton. 2000. IL-4 induces serine phosphorylation of the STAT6 transactivation domain in B lymphocytes. *Mol. Immunol.* 37: 641–652. [https://doi.org/10.1016/S0161-5890\(00\)00088-2](https://doi.org/10.1016/S0161-5890(00)00088-2)
- Yildiz, M., H. Li, D. Bernard, N.A. Amin, P. Ouillette, S. Jones, K. Saiya-Cork, B. Parkin, K. Jacobi, K. Shedden, et al. 2015. Activating STAT6 mutations in follicular lymphoma. *Blood.* 125:668–679. <https://doi.org/10.1182/blood-2014-06-582650>
- Zamò, A., J. Pischmarov, H. Horn, G. Ott, A. Rosenwald, and E. Leich. 2018. The exomic landscape of t(14;18)-negative diffuse follicular lymphoma with Ip36 deletion. *Br. J. Haematol.* 180:391–394. <https://doi.org/10.1111/bjh.15041>
- Zhang, Q., B. Boisson, V. Béziat, A. Puel, and J.L. Casanova. 2018. Human hyper-IgE syndrome: Singular or plural? *Mamm. Genome.* 29:603–617. <https://doi.org/10.1007/s00335-018-9767-2>
- Zhu, Z., Y. Guo, H. Shi, C.-L. Liu, R.A. Panganiban, W. Chung, L.J. O’Connor, B.E. Himes, S. Gazal, K. Hasegawa, et al. 2020. Shared genetic and experimental links between obesity-related traits and asthma subtypes in UK Biobank. *J. Allergy Clin. Immunol.* 145:537–549. <https://doi.org/10.1016/j.jaci.2019.09.035>
- Zhu, Z., P.H. Lee, M.D. Chaffin, W. Chung, P.-R. Loh, Q. Lu, D.C. Christiani, and L. Liang. 2018. A genome-wide cross-trait analysis from UK Biobank highlights the shared genetic architecture of asthma and allergic diseases. *Nat. Genet.* 50:857–864. <https://doi.org/10.1038/s41588-018-0121-0>
- Zhu, Z., X. Zhu, C.-L. Liu, H. Shi, S. Shen, Y. Yang, K. Hasegawa, C.A. Camargo Jr, and L. Liang. 2019. Shared genetics of asthma and mental health disorders: A large-scale genome-wide cross-trait analysis. *Eur. Respir. J.* 54:1901507. <https://doi.org/10.1183/13993003.01507-2019>

Supplemental material

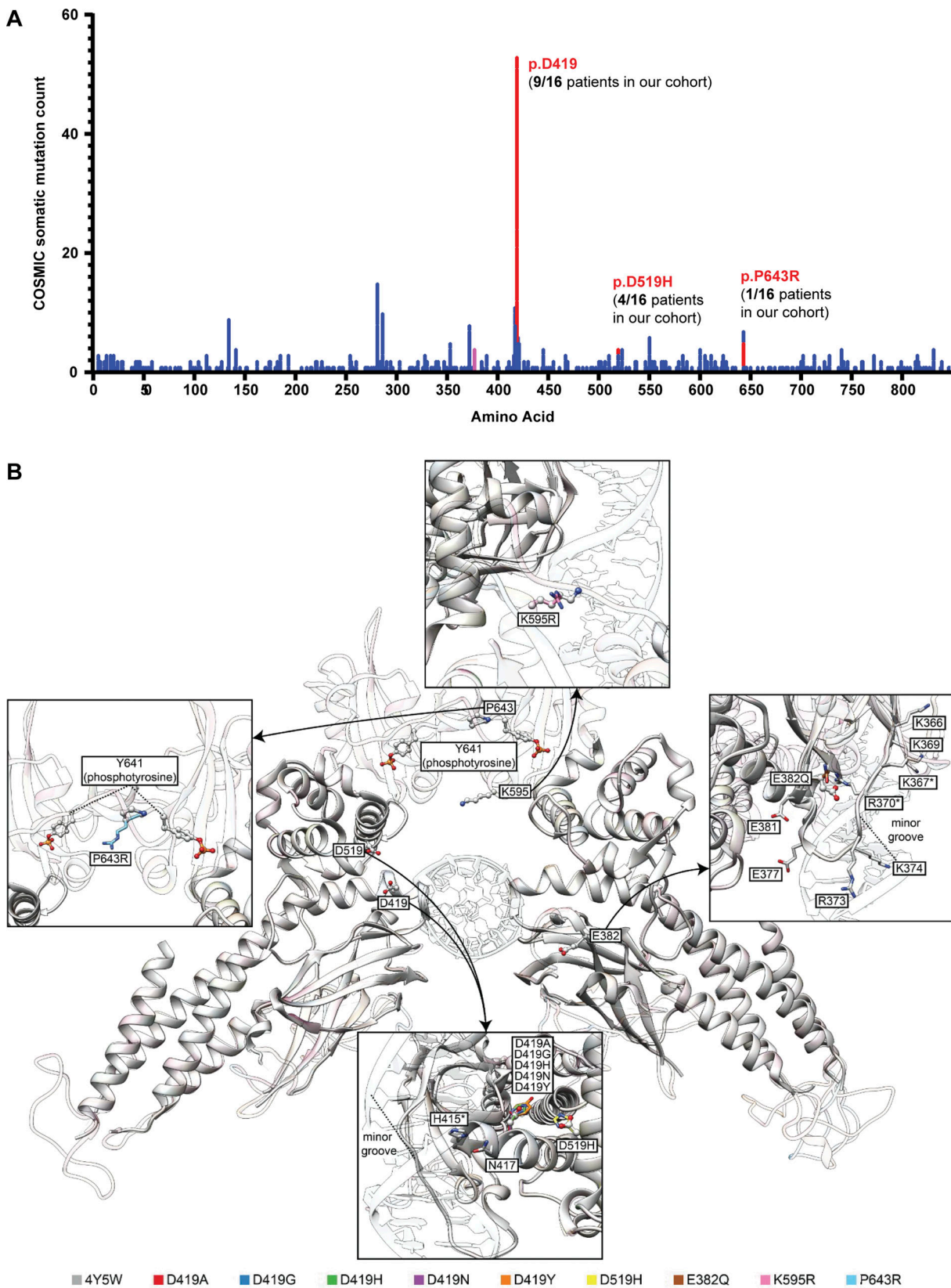


Figure S1. **Pathogenic STAT6 germline variants lie in different protein domains and are frequently identified as somatic variants.** (A) Somatic mutation counts for different amino acid changed as reported by COSMIC for STAT6. Red highlighted changes are those germline variants also identified in our cohort that cause severe allergic disease. (B) Structural model of the DNA-STAT6 homodimer complex showing location of the different STAT6 variants in relation to the DNA-binding interface. Specifically, zoom-ins for variants at each location are shown in relation to previously described variants known to affect STAT6 function.

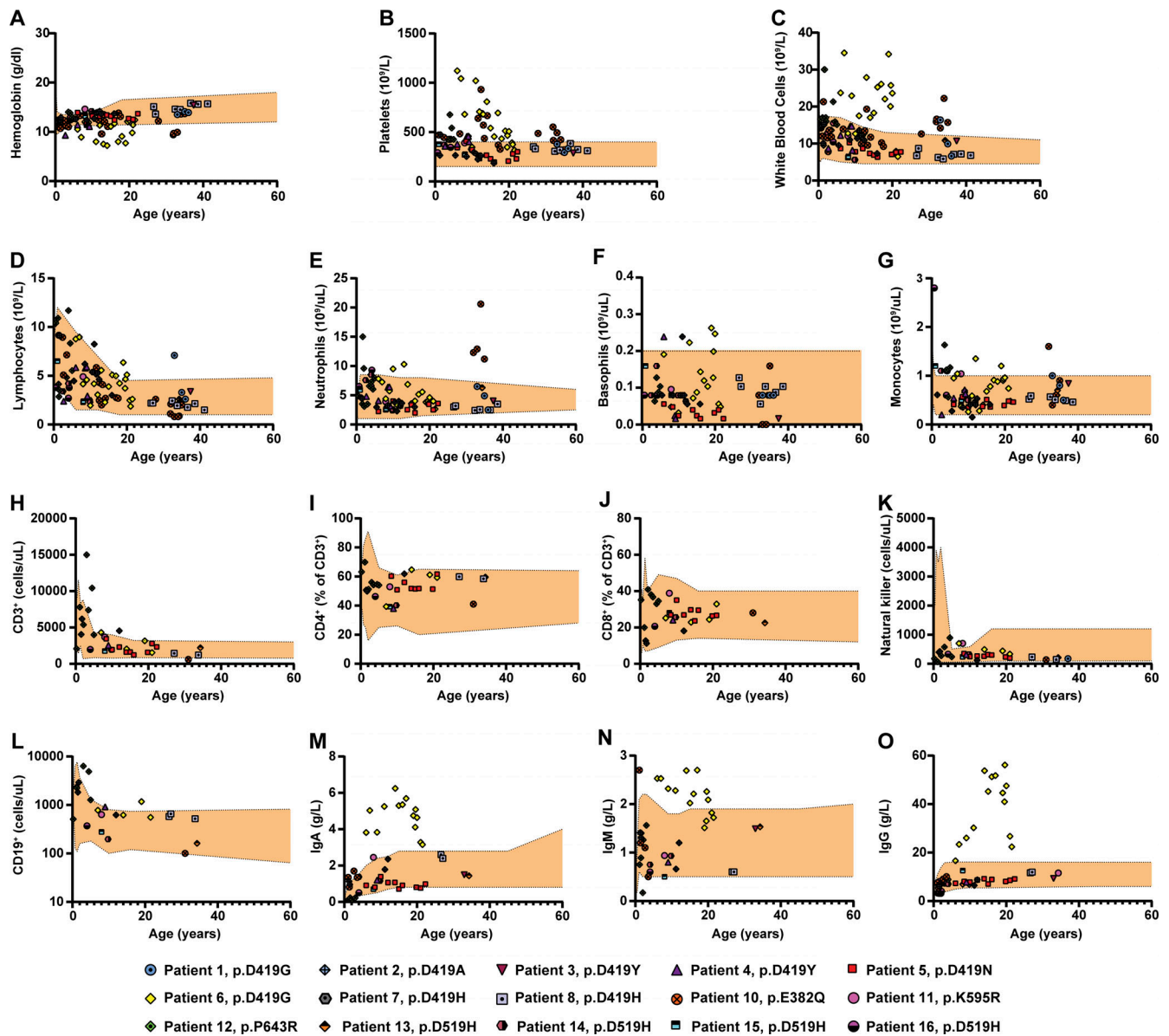


Figure S2. **Complete blood counts and immunological workup of patients with pathogenic STAT6 variants.** (A–G) Complete blood count for 15 out of the 16 patients and age-based references (orange-shaded area) for the following populations: (A) hemoglobin, (B) platelets, (C) white blood cells, (D) lymphocytes, (E) neutrophils, (F) basophils, and (G) monocytes. (H–L) Immunological workup for 15 out of the 16 patients showing age-based references (orange-shaded area) and populations quantification for: (H) CD3⁺ T cells, (I) CD4⁺ CD3⁺ T cells, (J) CD8⁺ CD3⁺ T cells, (K) NK cells, and (L) CD19⁺ B cells. (M–O) Immunoglobulin concentrations for 15 out of the 16 patients showing age-based references (orange-shaded area): (M) IgA, (N) IgM, and (O) IgG.

Downloaded from http://rupress.org/jem/article-pdf/220/5/e20221755/1448977/jem_20221755.pdf by Iran user on 14 March 2023

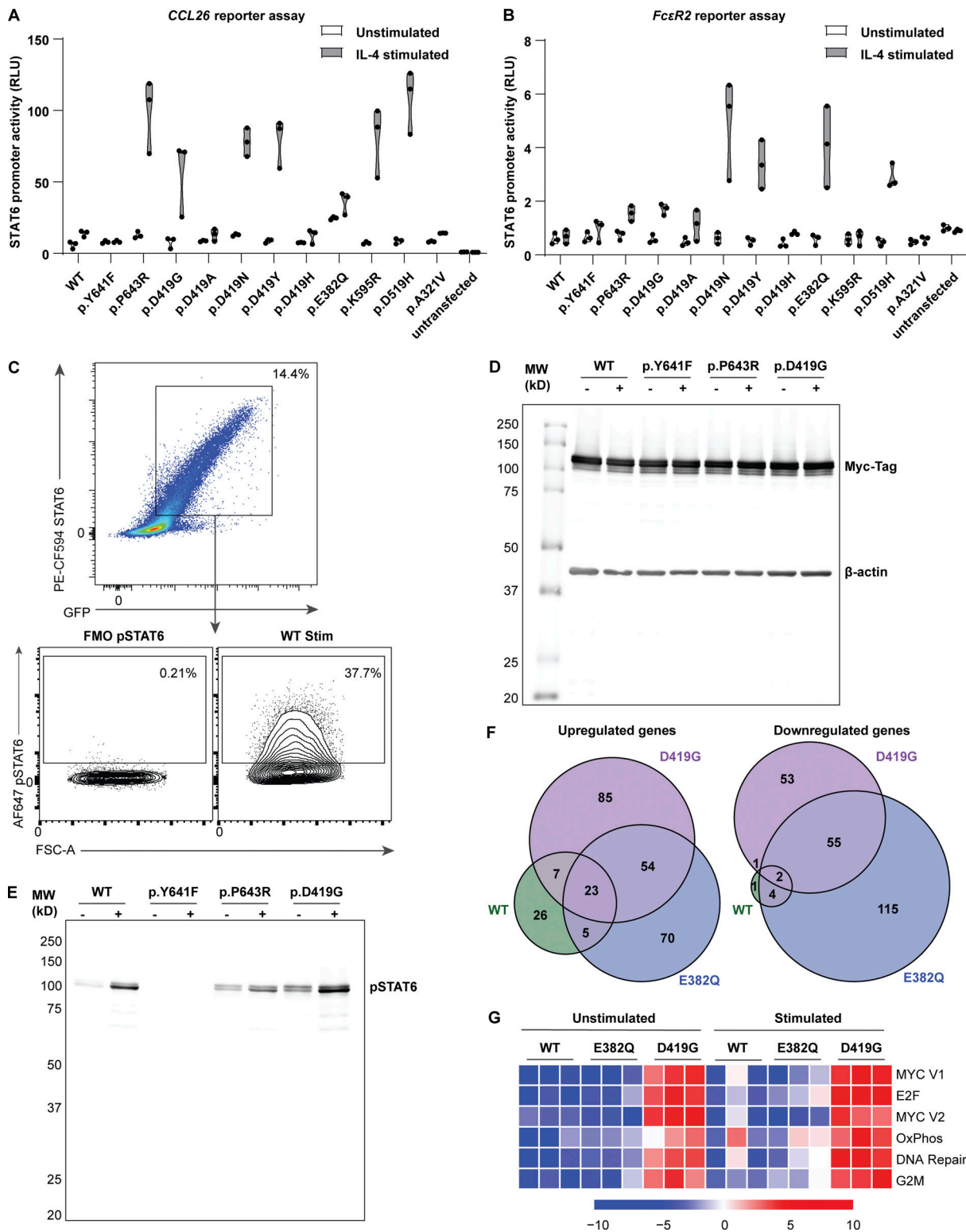


Figure S3. In vitro assays demonstrate that STAT6 variants lead to increased STAT6 activity. (A and B) Luciferase assay of STAT6 activity on a plasmid containing (A) *CCL26* promoter and (B) *FcεR2* promoter for WT-, different *STAT6*-variant transfected HEK293 cells before and after stimulation with IL-4 (100 ng/ml for 40 h), $n = 3$. (C) Gating strategy for determining % positive HEK293 pSTAT6 cells: dot plot for fluorescence minus one (FMO) is presented and was used for establishing pSTAT6⁺ cells. (D and E) Full-length immunoblots of the cropped immunoblots shown in Fig. 3 E, showing HEK293 cells transfected with WT-, inactive- (p.Y641F), p.P643R-, and p.D419G- *STAT6* variants for (D) Myc-tag and β -actin, as well as (E) pSTAT6 before and after treatment with IL-4 (10 ng/ml for 30 min). (F) Significantly upregulated (i) and downregulated (ii) genes upon IL-4 treatment in WT (green), p.E382Q (blue), and p.D419G (purple) in Jurkat cells as shown through Venn diagram. (G) Sample level enrichment analyses of significantly enriched immune pathways from MSigDB Hallmark in unstimulated and IL-4-stimulated samples, comparing WT vs. either p.E382Q or p.D419G. Heatmap is normalized across the rows and shown as relative expression.

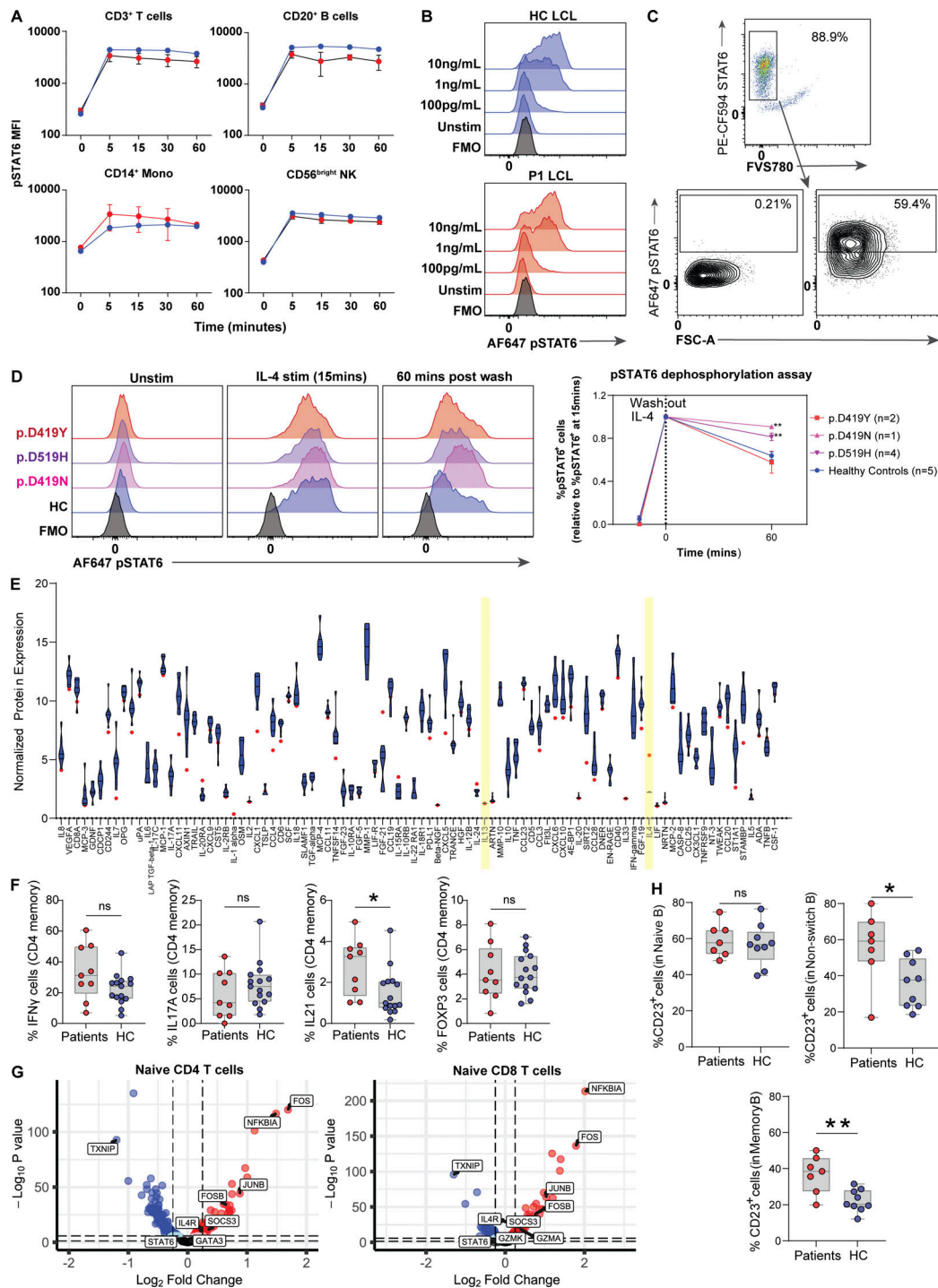


Figure S4. Measure of STAT6 activity in patient primary lymphocytes. (A) 1-h time course to measure phosphorylation of STAT6 in different populations of lymphocytes from five patients (red) and one healthy control (blue) after stimulation with IL-4 (10 ng/ml). (B) Dose response in LCLs of patient one (red) vs. one healthy control (blue) after stimulation of cells with various doses of IL-4 15 min. (C) Gating strategy to determine % pSTAT6 positive cells in LCLs: dot plot for FMO is presented and was used for establishing pSTAT6+ cells. (D) Histograms showing phosphorylation of STAT6 in healthy control (blue) and patients with genotype p.D419Y (red, n = 2), p.D519H (purple, n = 4), p.D419N (pink, n = 1), and healthy controls (blue, n = 5) in T cell blasts that were stimulated with IL-4 (10 ng/ml) for 15 min, washed with PBS, and subsequently incubated in IL-4-free media for 60 min. Quantification of pSTAT6+ cells is presented and normalized to max stimulation (noted at 15 min). Two-way ANOVA followed by Šidák's multiple comparisons was conducted. **, P < 0.01. (E) Readout of 92 biomarkers for P5 using throughput Olink proteomics. Eight healthy control distribution are shown as a violin plot in blue. The patient is shown as a red circle. Key cytokines, IL-4 and IL-13, are highlighted in yellow. (F) T helper cell distribution for nine patients (red) and 15 age-matched healthy controls (blue) each. (G) Transcriptomic comparison of naive CD4+ and naive CD8+ T cells between P6 and one healthy control measured through scRNAseq. Red genes are enriched in patient; blue genes are enriched in healthy control. The two dotted lines are the P value and adjusted P value respectively. (H) Quantification of % CD23 positive cells in naive, non-class switched memory, and class-switched memory B cells between patients (red, n = 7) and healthy controls (blue, n = 9) after stimulation with IL-4 (10 ng/ml) for 20 h. Unpaired t test. *, P < 0.05; **, P < 0.01.

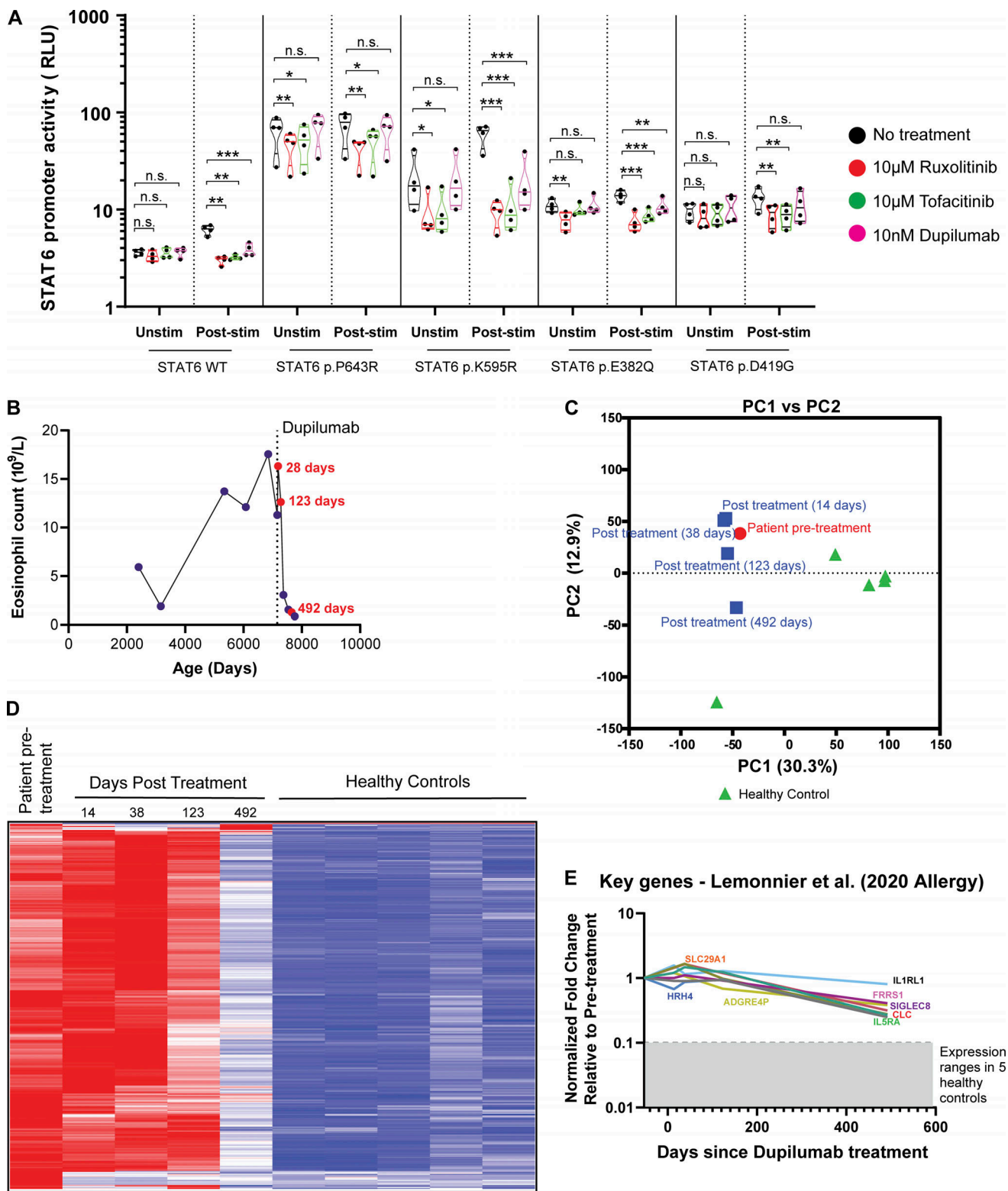


Figure S5. **STAT6 activity can be therapeutically targeted and can resolve clinical disease severity.** (A) Quantification of luciferase assay in HEK293 transfected cells pre-treated with ruxolitinib (10 μ M, 1 h), tofacitinib (10 μ M, 1 h), or dupilumab (10 nM, 1 h), before and after stimulation with IL-4 (0.02 ng/ml, 4 h). $n = 4$. One-way ANOVA and Tukey's post-hoc test. *, $P < 0.05$; **, $P < 0.01$; ***, $P < 0.001$. (B) Eosinophil counts before and following initiation of treatment with dupilumab are presented. Dots in red corresponds to transcriptomic data from this patient presented in Fig. 6 C. (C) PCA comparing whole blood bulk RNAseq of P6 before treatment with dupilumab and four time points after treatment, alongside five healthy controls. (D) Heatmap signatures of differentially expressed genes comparing pre-treatment patient samples against five healthy controls. Genes are row normalized. (E) Key genes, previously described to be biomarkers for allergic disease (Lemonnier et al., 2020) in whole blood RNA are presented for the patient samples. Gray shaded area is the range for the expression of these genes in five healthy controls.

Supplemental methods

Generation of STAT6 variant plasmids

Plasmids used for transfection studies contained full-length *STAT6* in a pCMV6 entry vector with a C-terminal GFP tag (Cat# RG210065; OriGene Technologies). To generate variants listed in Table S3, a Q5 site-directed mutagenesis kit (Cat# E0554S; New England Biolabs) was used according to the manufacturer's recommendations, with primer pairs noted in Table S1.

To generate lentivirus vectors, WT, p.E382Q, and p.D419G *STAT6* from the above plasmids were cloned into a GFP-tagged Lenti vector (Cat# PS100071; OriGene Technologies) using EcoRI-HF (Cat# R3101) and NotI-HF (Cat# R3189) both from New England Biolabs. The three *STAT6* plasmids were packaged using third-generation packaging plasmids and transfected into HEK293T cells. Culture media was collected, centrifuged, filtered, concentrated, and stored at -80°C before use.

All new variant plasmids were confirmed by Sanger sequencing and purified from 10-beta competent *E. coli* using a QIAprep Spin Miniprep Kit (Qiagen).

Transient and stable expression of STAT6 variants

Transient expression of *STAT6* variants in HEK293 cells were accomplished using a Lipofectamine 3000 kit (Thermo Fisher Scientific) according to the manufacturer's recommendations. Briefly, HEK293 cells were seeded at 2.0×10^5 cells/well in a 24-well plate in 0.5 ml of DMEM with 10% FBS (Gibco, Life Technologies) and incubated for 24 h at 37°C . Cells were transfected with 250 ng of plasmid DNA using the P3000 and Lipofectamine 3000 reagents and harvested after 24 h.

Stable expression of *STAT6* in Jurkat T cells was accomplished using the lentivirus approach as previously described (Kutner et al., 2009; Fung et al., 2021). Briefly, Jurkat T cells were infected with lentiviral particles in the presence of 5 $\mu\text{g/ml}$ polybrene (Sigma-Aldrich) and spinoculated at 800 *g* for 30 min at 32°C , cultured, and expanded in complete RPMI-1640 (GE Healthcare) supplemented with 10% FBS. Expanded cells were sorted on GFP expression using a BD FACS Aria (BD Biosciences) cell sorter.

Phospho-STAT6 detection in HEK293 cells

Phospho-*STAT6* activity was quantified by flow cytometry in transfected HEK293 cells stimulated with 10 ng/ml of IL-4 (Cat# 204-IL-020; R&D Systems) for 15 min or transfected cells pre-treated with either 10 μM ruxolitinib (Cat# trlr-rux; Invivogen), 10 μM tofacitinib (Cat# S50001; Selleckchem), or 10 nM dupilumab for 2 h before stimulation as previously described (Lu et al., 2021). Briefly, transfected and stimulated cells were fixed using BD Cytofix (Cat# 554655; BD Biosciences) for 20 min at 4°C and permeabilized using Perm III for 30 min on ice (Cat# 558050; BD Biosciences). The cells were then stained with *STAT6* PE-CF594 (Cat# 564148; BD Biosciences) and p-*STAT6* AF647 (Cat# 612601; BD Biosciences). p-*STAT6* expression was measured in GFP⁺*STAT6*⁺ cells from WT and *STAT6* variants samples on an LSRII flow cytometer (BD Biosciences) and analyzed using FlowJo software (BD Biosciences).

Phospho-STAT6 detection in PBMCs and T cell blasts

Freshly isolated PBMCs were rested for 1 h in RPMI medium (without FCS) at a final concentration of 0.5×10^6 cells/ml in a 96-well V-bottom plate. Cells were stained by Aqua Live/Dead Cell Stain Kit (Thermo Fisher Scientific; DCM; 10 min in 37°C). After removing the DCM by washing with RPMI, cells were left unstimulated or were stimulated with IL4 (100 ng/ μl) at different time points (0 min, 5 min, 15 min, 30 min, 60 min in 37°C). After the desired time point stimulation, the cells were fixed by adding 100 μl of prewarmed BD Phosflow Fix Buffer I (BDB557870) directly to the wells (10 min in 37°C). Then cells were washed with 200 μl FACS buffer (PBS + 2% DMSO + 2 mM EDTA) and permeabilized in 100 μl of cold BD Phosflow Perm Buffer III (Cat# 558050) for 20 min at 4°C . The cells were washed two times with 200 μl FACS buffer and stained using a cocktail of antibodies (Table S2) for 60 min at room temperature and darkness. Samples were acquired on a FACS Gallios machine.

For the generation of T cells blasts, T cells were first isolated from PBMCs using EasySep Human T Cell Isolation Kit (Cat# 17951; Stemcell). Subsequently, the cells were treated with exogenous IL-2 (100 U/ml) and ImmunoCult Human CD3/CD28 T cell Activator (Cat# 10971; Stemcell) for 12 d and maintained at a concentration of 1 million cells/ml every 2 d. Phosphorylation and dephosphorylation of *STAT6* was measured as described above at time points: 0, 15 min of IL-4 stimulation (10 ng/ml), and 60 min after wash out of IL-4. The following antibodies were used: *STAT6* PE-CF594 (Cat# 564148; BD Biosciences), p-*STAT6* AF647 (Cat# 612601; BD Biosciences), and Fixable Viability Stain 780 (Cat# 565388; BD Biosciences). Samples were acquired on the BD FACSymphony.

Intracellular cytokine staining on patient PBMCs

To carry out intracellular cytokine detection/ T_H phenotyping, PBMCs from the patient and five age-matched controls were stimulated with PMA/ionomycin for 4 h at 37°C in the presence of GolgiStop (Cat# 554724; BD Biosciences). Cells were stained with an antibody panel (Table S3) using the eBioscience Foxp3 Transcription Factor Staining Buffer Set (Cat# 00-5523-00; Invitrogen, Thermo Fisher Scientific). Samples were acquired on the BD FACSymphony flow cytometer (BD Biosciences). Data were analyzed using FlowJo (BD Biosciences).

Olink high-throughput proteomics

Serum proteins for P5 were analyzed using a multiplex technology based on proximity-extension assays (Lundberg et al., 2011). We measured specific proteins using the Olink panel of inflammation. Briefly, the kit consisted of a microtiter plate for measuring 92 protein biomarkers in 88 samples, and each well contained 96 pairs of DNA-labeled antibody probes. To minimize inter- and intra-run variation, the data were normalized using both an internal control (extension control) and an inter-plate control, and then transformed using a pre-determined correction factor. The pre-processed data were reported in arbitrary units as normalized protein expression (NPX) that enables individual protein analysis across a sample set analyzed in log₂ scale, wherein a higher NPX correlates with higher protein expression. The data were pre-processed using the NPX Manager Software and OlinkAnalyze R package (v1.3.0). The data for two key T_H2 cytokines, IL-4 and IL-13, are highlighted in Fig. S4 E.

CD23 and IL-4Rα staining on lymphocytes

Expression of IL-4Rα and CD23 was studied on primary patient B cells (within PBMCs). Briefly, primary patient cells were incubated in RPMI with or without IL-4 (10 ng/ml). After 20 h, the cells were washed and stained with the following antibodies: BV510 mouse anti-human CD3 (Cat# 563109; BD; clone: UCHT1), APC-R700 mouse anti-human CD4 (Cat# 565995; BD; clone: SK3), BUV395 mouse anti-human CD8 (Cat# 740303; BD; clone: HIT8a), BUV737 mouse anti-human CD19 (Cat# 741829; BD; clone: HIB19), BV786 mouse anti-human CD27 (Cat# 563328; BD; clone: L128), PerCP-Cy5.5 mouse anti-human CD45RA (Cat# 563429; BD; clone: HI100), BV605 mouse anti-human IgD (Cat# 563313; BD; clone: IA6-2), BB515 mouse anti-human IgM (Cat# 564622; BD; clone: G20-127), BV421 mouse anti-human CD23 (Cat# 562707; BD, clone: M-L233), PE mouse anti-human CD124 (IL-4Rα; Cat# 355003; BioLegend; clone: G077F6), and Fixable Viability Stain 780 (Cat# 565388; BD). Cells were acquired on the BD FACSymphony.

Luciferase reporter assays with 4× STAT6 binding sites

A luciferase reporter plasmid encoding a 4× STAT6 binding site (TTCCCAAGAA) was used to assess WT and variant STAT6 promoter activity (Li et al., 2016). The p4xSTAT6-Luc2P plasmid (Addgene plasmid #35554; Addgene; <http://n2t.net/addgene:35554>; RRID: Addgene_35554) was a gift from Axel Nohturfft (St. George's University of London, London, UK). Briefly, HEK293 cells were seeded in 24-well plates overnight at a density of 200,000 cells and transfected with 250 ng of p4xSTAT6-Luc2P, 250 ng of a plasmid encoding a GFP-tagged WT or variant STAT6, and 10 ng Renilla luciferase (R-Luc) using Lipofectamine 3000. Transfected cells were subsequently stimulated with 0.2 ng/ml of IL-4 (Cat# 6507-IL-010; R&D Systems) or left unstimulated. Additionally, for inhibitor assays, transfected cells were incubated with either 10 μM ruxolitinib (Cat# tlr-rux, Invivogen), 10 μM tofacitinib (Cat# S50001; Selleckchem), or 10 nM dupilumab (Cat# HY-P9926; MedChemExpress) for 1 h before stimulation. Cell lysates were prepared and processed using a Dual-Glo Luciferase Assay Kit (Cat# E2920; Promega) according to the manufacturer's recommendations. Luciferase activity was measured on the Infinite M200 plate reader (Tecan).

Luciferase reporter assay with CCL26 and FcεR2 promoter

Luciferase reporter plasmids with CCL26 and FcεR2 promoter were also used to study STAT6 activity and were constructed from pMCS-Gaussia Dura Luc vector (#16190; ThermoFisher Scientific). 293FT cells (#51-0035; Invitrogen) were seeded in 24-well plates overnight at a density of 200,000 cells and transfected with 245 ng of pCCL26/pFcεR2V2-Gaussia Dura Luc, 245 ng of a plasmid encoding WT and variant STAT6, and 10 ng pCMV-red firefly Luc vector (#16156; ThermoFisher Scientific) using TransIT-2020 transfection reagent (#MIR5400; Mirus). Transfected cells were subsequently stimulated with 100 ng/ml of IL-4 (#200-04; Pe-protech) or left untreated. Cell lysates were prepared and processed using Pierce Gaussia-Firefly Luciferase Dual Assay Kit (#16182; Thermo Fisher Scientific) according to the manufacturer's recommendations. Luciferase activity was measured on the luminometer (Fusion alpha-FP, PerkinElmer Packard), and signals of Gaussia luciferase were normalized to those of red firefly luciferase.

Whole blood RNAseq

Human peripheral blood was collected in EDTA tubes. Erythrocytes were removed with RBC Lysis Solution (#158904; Qiagen) and the resultant white cell pellet was washed once with PBS. RNA was extracted with TRIzol (#15596026; Ambion). Library preparation and Illumina sequencing (pair-end sequencing of 151 bp) were done at the Genomics Core of the Centre for PanorOmic Sciences in LKS Faculty of Medicine of The University of Hong Kong. Complementary DNA (cDNA) libraries were prepared by KAPA mRNA HyperPrep Kit KR1352-v3.16 (#08098123702; Roche). One microgram of total RNA was used as starting material. The manufacturer's protocol was followed. In brief, poly-A containing mRNA was collected using poly-T oligo-attached magnetic beads. The purified mRNA was fragmented to 200–300 bp by incubating at 94°C for 6 min in the presence of magnesium ions. The fragmented mRNA was then applied as template to synthesize the first-strand cDNA using random hexamer-primer and reverse transcriptase. In the second strand cDNA synthesis, the mRNA template was removed and a replacement strand was generated to form the blunt-end double-stranded (ds) cDNA. The ds-cDNA underwent 3' adenylation and ligation with xGen Dual Index UMI Adapters (Integrated DNA Technologies). The adaptor-ligated libraries were enriched by 10 cycles of PCR. The libraries were denatured and diluted to optimal concentration. Illumina NovaSeq 6000 was used for pair-end 151 bp sequencing.

De-multiplexed read sequences were aligned to a reference sequence and transcript expression were estimated using the DRAGEN RNA pipeline on Illumina Basespace. Expression data was normalized to reads between samples using the edgeR package in R (R Foundation). Normalized counts were filtered to remove low counts using the filterByExpr function in edgeR (Chen et al., 2016). PCA was done on $\log_2(\text{normalized counts}+0.25)$ in R using the PCA function. Differential expression was conducted using Limma (Ritchie et al., 2015), on patient pre-treatment sample against 5 healthy controls. Differentially expressed genes (adjusted P value <0.05) were visualized using pheatmap in R. Cell type abundance was estimated using the LM22 signature matrix file in Cibersort (Newman et al., 2015). Cell types were reduced to nine immunologically relevant cell types: neutrophils, eosinophils, mast cells, dendritic cells, monocytes, NK cells, CD4 T cells, CD8 T cells, memory B cells, and naive B cells. Raw data are deposited in the Gene Expression Omnibus with accession number GSE215390.

Jurkat RNAseq

RNA was extracted in triplicate as previously described (Lu et al., 2021) using a RNeasy Mini Plus Kit (Qiagen) according to the manufacturer's recommendations. RNA was prepared following the standard protocol for the NEBNext Ultra II Stranded mRNA (New England Biolabs) and sequenced on the Illumina NextSeq 500 with Paired End 42×42 bp reads. De-multiplexed read sequences were aligned to a reference sequence using RNA-Seq Alignment app (v1.1.1) on Illumina Basespace, using Spliced Transcripts Alignment to a Reference (STAR) aligner and Cufflinks 2 for assembly and estimation of gene expression.

Expression data were normalized to reads between samples using the edgeR package in R (R Foundation). Normalized counts were filtered to remove low counts using the filterByExpr function in edgeR (Chen et al., 2016). PCA was done on $\log_2(\text{normalized counts}+0.25)$ in R using the PCA function. Differential expression between unstimulated and stimulated samples for all three STAT6-transduced Jurkat T cells was accomplished using Limma (Ritchie et al., 2015). Differentially expressed genes were defined as those with fold change (FC) >1.25 and adjusted P value <0.05 .

Pathway analysis was done by first performing GSEA with 1,000 permutations using the Molecular Signatures Database Hallmark module. Signal-to-noise ratio was used for gene ranking and the obtained normalized enrichment scores and P values were further adjusted using the Benjamini-Hochberg method. Pathways with an adjusted P value <0.05 were considered significant. Leading-edge genes from significant pathways between STAT6 WT and STAT6 c.1256A>G Jurkat were identified (no significantly upregulated pathways were identified between STAT6 WT and STAT6 c.1144G>C). Expression levels of these genes were then determined in each of the three groups (WT, c.1144G>C, c.1256A>G) under both stimulated and unstimulated conditions. Sample level enrichment analyses scores were computed as previously described (Kulpa et al., 2019). Briefly, z-scores were computed for gene sets of interest for each sample. The mean expression levels of significant genes were compared to the expression of 1,000 random gene sets of the same size. The difference between observed and expected mean expression was then calculated and represented on heatmaps.

GSEA was also done on two other gene sets: (i) STAT6 targets and (ii) IL-4 T_H2 targets. STAT6 targets were defined as the set of genes that were significantly upregulated upon IL-4 stimulation in WT-STAT6-transduced Jurkat T cells. Enrichment of this gene set was determined at both baseline and after IL-4 stimulation between WT and p.E382Q STAT6, and WT and p.D419G STAT6 Jurkat T cells. IL-4-STAT6 T_H2 skewing targets were previously reported (Elo et al., 2010) STAT6 target genes that are significantly upregulated in response to IL-4 treatment and that lead to T_H2 skewing. Raw data are deposited in the Gene Expression Omnibus with accession number GSE222646.

Western blot

Cell lysates were prepared by lysis of HEK293 cells in a modified radio immunoprecipitation assay buffer with the Halt protease and phosphatase inhibitors cocktail (Thermo Fisher Scientific). Cell lysates were separated by 10% SDS-PAGE and transferred onto polyvinylidene difluoride membranes (Immobilon-FL; MilliporeSigma). Membranes were blocked with 5% BSA in Tris-buffered saline with Tween-20, incubated with primary antibodies for 18 h at 4°C, incubated with secondary antibodies for 1 h at room temperature, and imaged using a LI-COR Odyssey infrared scanner (LI-COR Biosciences). The primary antibodies used were the following: STAT6 (Cat# 9362), pSTAT6 (Cat# 9361), Myc-tag (Cat# 2276), and β -actin (Cat# 3700), all from Cell Signaling Technologies. The secondary antibodies used were the following: goat anti-rabbit IgG DyLight 800 conjugated (611-145-002-0.5; Rockland Immunochemicals) and goat anti-mouse IgG IRDye 680RD (926-6870; LI-COR).

scRNAseq

scRNAseq was done on a patient sample before and after dupilumab treatment along with one age-matched healthy control. Human peripheral blood was collected in lithium heparin tubes and PBMCs were isolated using Lymphoprep (AS #04-03-9391/02; Alere Technologies). Single-cell suspension was obtained by passing through a 30 μm Pre-Separation Filter (#130-041-407; Miltenyi Biotec GmbH). Dead cells were removed by Dead Cell Removal Kit (#130-090-101; Miltenyi Biotec GmbH). T cell isolation was performed using Pan T cell Isolation Kit (#130-096-535; Miltenyi Biotec GmbH). Single-cell encapsulation and library preparation are done at Genomics Core of the Centre for PanorOmic Sciences in LKS Faculty of Medicine of The University of Hong Kong. Single cell encapsulation and cDNA libraries were prepared by Chromium Single Cell 5' Reagent Kit v1 and Chromium Single Cell A Chip Kit, or by Chromium Next GEM (gel beads-in-emulsion) Single Cell 5' Reagent Kit v2 (Dual Index) and Chromium Next GEM Chip K Single Cell

Kit. Cells in suspension were counted and loaded into individual wells of 10X Chromium Single Cell chip (10X Genomics). Single cells were then encapsulated into GEM by 10X Chromium Single Cell Controller. Single Cell 5' Reagent Kit was used to perform downstream steps: reverse transcription is performed on GEMs, followed by cDNA clean-up and amplification. The ds-cDNA went through enzymatic fragmentation and adapter ligation. Index PCR and SPRIselect size selection were then done as per the manufacturer's protocol. Library size and concentration are determined by Qubit, quantitative PCR, and Bioanalyzer assays. The libraries were denatured and diluted to optimal concentration. Illumina NovaSeq 6000 was used for pair-end 151 bp sequencing with NovaSeq 6000 S4 Reagent Kit v1.0 and v1.5 (#20012866 and #20028312; Illumina).

The raw FASTQ data was obtained, and the cellranger count function was then applied to generate single cell feature counts for every single library (Cell Ranger v5.0.1). The output of filtered feature-barcode matrix containing only detected cell-associated barcodes was used for further downstream analysis. The default parameters and options were applied for cellranger count after providing the input FASTQ data and the relevant prebuilt references of the Human dataset (GRCh38) downloaded from the 10X Genomic website (<https://support.10xgenomics.com/single-cell-gene-expression/software/downloads/latest/>).

The filtered expression matrix generated by Cell Ranger for each sample was analyzed and processed with the R package Seurat (v3.2.0). Quality control involved first filtering for quality based on the following criteria: mapping to over 200 unique genes, the fraction of mitochondrial transcripts was <10%, and the fraction of unique hemoglobin transcripts was <1%. Scaling and clustering was performed on PBMCs and enriched T cells separately. Dimensionality reduction using PCA was done on the 2,000 most variable genes and UMAP was based on the first 20 PCs. Cell identities were first annotated with SingleR using fine labeling from the Novershtern hematopoietic dataset (Novershtern et al., 2011; Aran et al., 2019) and Monaco Immune dataset (Monaco et al., 2019) for PBMCs and enriched T cells respectively. The annotation was refined manually based on the UMAP clustering patterns, grouping the SingleR labels for PBMCs into 10 main populations: naive B cells, memory B cells, naive CD4⁺, memory CD4⁺, naive CD8⁺, memory CD8⁺, monocytes, dendritic cells, NK cells, and others. For differential gene expression analyses, we utilized the Seurat implementation of negative binomial test, assuming an underlying negative binomial distribution in RNAseq data (Robinson and Smyth, 2007; Hafemeister and Satija, 2019).

All the computational resources were obtained from the cluster of High Performance Computing Facility of the Centre for PanorOmic Sciences, University of Hong Kong. Raw data are deposited in the Gene Expression Omnibus with accession number GSE215405.

NIHR BioResource Rare Diseases PID Consortium members

Zoe Adhya, Hana Alachkar, Ariharan Anantharachagan, Richard Antrobus, Gururaj Arumugakani, Chiara Bacchelli, Helen Baxendale, Claire Bethune, Shahnaz Bibi, Barbara Boardman, Claire Booth, Michael Browning, Mary Brownlie, Siobhan Burns, Anita Chandra, Hayley Clifford, Nichola Cooper, Sophie Davies, John Dempster, Lisa Devlin, Rainer Doffinger, Elizabeth Drewe, David Edgar, William Egner, Tariq El-Shanawany, Bobby Gaspar, Rohit Ghurye, Kimberley Gilmour, Sarah Goddard, Pavel Gordins, Sofia Grigoriadou, Scott Hackett, Rosie Hague, Lorraine Harper, Grant Hayman, Archana Herwadkar, Stephen Hughes, Aarnoud Huissoon, Stephen Jolles, Julie Jones, Peter Kelleher, Nigel Klein, Taco Kuijpers (principal investigator), Dinakantha Kumararatne, James Laffan, Hana Lango Allen, Sara Lear, Hilary Longhurst, Lorena Lorenzo, Jesmeen Maimaris, Ania Manson, Elizabeth McDermott, Hazel Millar, Anoop Mistry, Valerie Morrisson, Sai Murng, Iman Nasir, Sergey Nejentsev, Sadia Noorani, Eric Oksenhendler, Mark Ponsford, Waseem Qasim, Ellen Quinn, Isabella Quinti, Alex Richter, Crina Samarghitean, Ravishankar Sargur, Sinisa Savic, Suranjith Seneviratne, Carrock Sewall, Fiona Shackley, Ilenia Simeoni, Kenneth G.C. Smith (principal investigator), Emily Staples, Hans Stauss, Cathal Steele, James Thaventhiran, Moira Thomas, Adrian Thrasher (principal investigator), Steve Welch, Lisa Willcocks, Sarita Workman, Austen Worth, Nigel Yeatman, and Patrick Yong.

Provided online are Table S1, Table S2, Table S3, Table S4, Table S5, Table S6, Table S7, and Data S1. Table S1 lists primers used for site-directed mutagenesis. Table S2 lists antibodies used for phospho-flow on different immune subsets. Table S3 lists antibodies used for T_H phenotyping in patient PBMCs. Table S4 shows variant annotation and pathogenicity prediction of the variants reported within the DNA-binding domain of STAT6 for 10 patients. Table S5 shows variant annotation and pathogenicity prediction of the variants reported outside of the DNA-binding domain of STAT6 for six patients. Table S6 lists genes upregulated (gray) and downregulated (red) in transduced WT-, p.E382Q-, and p.D419G-transduced Jurkats that meet the cutoff of fold-change (FC) > 1.25 and adjusted P value < 0.05. Table S7 lists genes in the leading edge driving the enrichment of two pathways (IL-4/STAT6 pathway and T_H2 pathway) between transduced WT- vs. p.E382Q- and WT- vs. p.D419G- Jurkats. Data S1 describes clinical narratives for each patient.